Interaction of oxygen with Al(111) studied by scanning tunneling microscopy

H. Brune, J. Wintterlin, J. Trost, and G. Ertl
Fritz-Haber-Institut der Max-Planck-Gesellschaft, Faradayweg 4-6, D-14195 Berlin, Germany

J. Wiechers and R. J. Behm
Abt. für Oberflächenchemie und Katalyse, Universität Ulm, D-89069 Ulm, Germany

The interaction of oxygen with Al(111) was studied by scanning tunneling microscopy (STM). Chemisorbed oxygen and surface oxides can be distinguished in STM images, where for moderate tunnel currents and independent of the bias voltage the former are imaged as depressions, while the latter appear as protrusions. An absolute coverage scale was established by counting O adatoms. The initial sticking coefficient is determined to $s_0 = 0.005$. Upon chemisorption at 300 K the O adlayer is characterized by randomly distributed, immobile, individual O adatoms and, for higher coverages, by small (1×1) O islands which consist of few adatoms only. From the random distribution of the thermalized O adatoms at low coverages a mobile atomic precursor species is concluded to exist, which results from an internal energy transfer during dissociative adsorption. These "hot adatoms" "fly apart" by at least 80 Å, before their excess energy is dissipated. A model is derived which explains the unusual island nucleation scheme by trapping of the hot adatoms at already thermalized oxygen atoms. Oxidation starts long before saturation of the (1×1) O adlayer, at coverages around $\Theta_O \cong 0.2$. For a wide coverage range bare and O_{ad} covered surfaces coexist with the surface oxide phase. Upon further oxygen uptake both chemisorbed and oxide phase grow in coverage. Oxide nucleation takes place at the interface of O_{ad} islands and bare surface, with a slight preference for nucleation at upper terrace step edges. Further oxide formation progresses by nucleation of additional oxide grains rather than by growth of existing ones, until the surface is filled up with a layer of small oxide particles of about 20 Å in diameter. At very large exposures up to 5×10^5 L they cover the entire surface as a relatively smooth, amorphous layer of aluminum oxide. The difference in Al atom density between Al metal and surface oxide is accommodated by short range processes, with no indication for any long range Al mass transport. Based on our data we discuss a simpler two step model for the interaction of oxygen with Al(111), without making use of an additional subsurface oxygen species. The complex spectroscopic data for the O/Al(111) system are rationalized by the wide coexistence range of bare and O_{ad} covered surface with surface oxide and by differences in the electronic and vibronic properties of the surface atoms depending on the number of neighboring O adatoms in the small O_{ad} islands.

I. INTRODUCTION

Because of its enormous practical importance, the oxidation of metal surfaces has been studied intensively for many years.[1] Particular attention has been paid to the initial stages of the reaction, the so-called "induction period," preceding the later thickness growth of the oxide. It is generally accepted that this includes a number of different processes such as dissociation of the oxygen molecules on the bare surface, the formation of a chemisorbed layer, and finally nucleation of the oxide. In most cases, however, the actual reaction is even more complex. Oxygen often forms more than one chemisorbed phase or can diffuse into deeper layers, or the surface may reconstruct. (See, e.g., the review on the interaction of oxygen with some transition metals.[1]) Not surprisingly, despite of considerable experimental and theoretical efforts the mechanistic understanding of the oxidation process, on an atomic scale, is still not very far developed, and a common reaction pattern could not be identified so far.

Because of its apparent simplicity the interaction of oxygen with Al(111) had for some time been considered to represent a model system for the oxidation of metal surfaces. This would have allowed to study the basic steps of the oxidation induction period such as the O_2 dissociation without complicating rearrangement effects on the surface. Early studies using x-ray photoelectron spectroscopy (XPS) and low energy electron diffraction (LEED)[2] suggested the existence of an ordered overlayer of dissociatively adsorbed atomic oxygen, arranged in a (1×1) lattice. The O_{ad} covered surface was characterized by a shift of the Al($2p$) core level of 1.4 eV to higher binding energy and a (1×1) LEED pattern with sharp diffraction spots. Significant changes in the LEED intensity-voltage curves indicated that the (1×1) pattern was predominantly due to an ordered (1×1) oxygen adlayer and not to the substrate alone.[2] From surface extended x-ray absorption fine structure (SEXAFS) measurements an oxygen–aluminum distance of 1.76–1.79 Å was determined for this phase,[3,4] corresponding to a vertical distance of the oxygen atom to the topmost metal layer of only 0.6–0.7 Å. This value was

based on the assumption of a threefold-hollow surface site, for which, however, there existed no direct evidence. Upon further increasing the oxygen exposure aluminum oxide was found to form at the surface. Main evidence for this assignment was an energy shift of the Al($2p$) state by 2.7 eV to higher binding energy as compared to its position on the clean metal,[2] which is identical to the energy observed in bulk aluminum oxide,[5] or the appearance of additional Al(LVV) transitions in Auger electron spectra (AES) with a dominant peak around 54 eV.[6] From these results a simple reaction scheme was concluded, whereafter in a first reaction step the surface is covered by a (1×1) oxygen adlayer, before the actual oxidation of the surface region proceeds in a second step. The disappearance of the (1×1) spot intensity in the LEED pattern during oxidation at room temperature suggested that in the later stages of oxidation the Al substrate is completely covered by an amorphous oxide layer. The nearly free electron character of aluminum made the (1×1) chemisorbed oxygen layer on the (111) surface also a favorite system for theoretical studies of adsorption.[7]

Later experimental results, however, were inconsistent with the initially proposed reaction scheme. The changes in work function in the chemisorption regime were found to be anomalously small, around 0.1 to 0.2 eV,[6,8–12] with some authors even reporting an initial decrease upon oxygen adsorption.[8,9] This contrasts with the usual behavior observed on most metal surfaces, where the dipole moment formed by the adsorbed, electronegative oxygen atoms leads to a significant increase in work function. To account for this observation the idea of a subsurface site of oxygen was put forward. High resolution electron energy loss spectroscopy (HREELS)[3,13,14] pointed to an even more complex mechanism. Multiple loss peak spectra were found in the chemisorption regime, whereas a single vibrational mode would have been expected for a (1×1) overlayer with oxygen on a single adsorption site. The spectra were mostly interpreted in terms of a modified reaction scheme in which from the beginning on two different adsorption sites are occupied by oxygen atoms, a surface and a subsurface site. Very recent standing x-ray absorption experiments,[15] which found the chemisorbed oxygen atoms to reside on fcc type threefold hollow sites, again supported a single adsorption site (*on* the surface) and lent credit to the SEXAFS results mentioned before. Finally in an Al core level photoemission study[16] it was shown that the island structure of the oxygen adlayer may be important for the understanding of the complex experimental data and hence has to be taken into consideration.

The conflict on the O adsorption site, and in particular on mechanistic aspects of oxygen chemisorption and the beginning oxide formation has still not been resolved, although the reaction has now been studied by almost the complete variety of surface analytical techniques. It was also addressed in some of the theoretical investigations (see the review[7]). Of course, the structure of the chemisorbed layer will be crucial for the subsequent transformation into the oxide, because this step necessarily includes the interdiffusion of metal and oxygen atoms.

In an attempt to gain more direct insight into this confusing situation we have initiated a scanning tunneling microscopy (STM) study on the interaction of oxygen with the Al(111) surface. Our main objective is a detailed description of the adsorption and reaction mechanism up to the oxidation regime. The results of this study will be presented in two parts. The first, present one will cover the adsorption behavior and the onset of oxidation at room temperature conditions. This part also contains a brief discussion of the imaging of adsorbed oxygen atoms on this surface by STM. Observations made after treatment at elevated temperatures will be reported later. For room temperature adsorption we find a simple reaction scheme for the interaction of oxygen with Al(111), where (dissociative) adsorption occurs in a first step, leading to an adlayer which consists of randomly distributed individual adatoms at lowest coverages and of an increasing number of small (1×1) islands at higher coverages. From the distribution of oxygen atoms we are able to infer details of the dynamics of the dissociation process. Nucleation of small oxide nuclei proceeds long before the adsorption process is completed, with a small but noticeable preference for oxide nucleation at step edges. Hence clean surface, chemisorbed oxygen and oxide nuclei coexist over a wide coverage range. In contrast to former interpretations we find a single chemisorption state only. The complexity of spectroscopic data is attributed to the operation of (substrate mediated) interactions between oxygen adatoms on neighboring adsorption sites, which lead to significant modifications of the electronic and vibronic properties of adatoms depending on the number of O_{ad} neighbors, i.e., whether they exist as individual adatoms, at the perimeter of adatom islands or in the inner part of these islands. This interpretation agrees well with conclusions drawn from high resolution Al ($2p$) spectra[16] and from a combined theoretical and experimental study on the energy of O($1s$) core levels, which appeared during preparation of this manuscript.[17,18]

We will start here with a description of the experimental setup and procedures and of the sample preparation in Sec. II. The following Sec. III begins with an overview over structural characteristics of clean Al(111) surfaces in Sec. III A where we compare these data also with images of slightly contaminated surfaces. Measurements on the representation of adsorbed oxygen in STM images and its variation with bias voltage and tunnel current are presented in Sec. III B. We then focus on structural effects and structural results of oxygen adsorption in the chemisorption regime, before the onset of oxide nucleation. These are described in Sec. III C. A report on the existence of hot oxygen adatoms, indicative of an energy transfer during the dissociative chemisorption process into kinetic energy of the individual adatoms, has been published earlier.[19] The onset of oxidation is described in the last subsection (III D) in this section. This includes data on the nucleation and growth of oxide nuclei as well as on the overall development of the surface topography during the initial stages of oxidation. Finally, in Sec. IV the results are discussed in comparison with existing data from the literature.
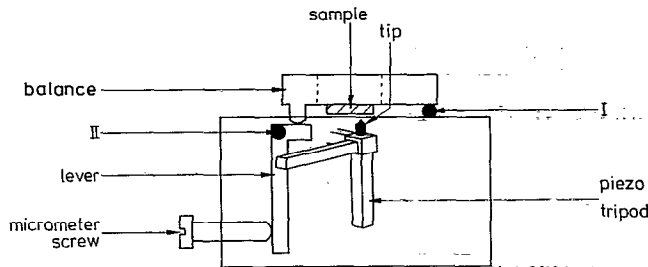
FIG. 1. Schematic drawing of the STM, showing the essential parts of the coarse approach mechanics. The block is the microscope body, which contains the piezo tripod, an L-shaped lever, and a micrometer screw. The cover on the top is a balance with the rotatable sample.

II. EXPERIMENT

The experiments were performed with an STM of the so-called "pocket size" type, where a high mechanical stability is achieved by small size and hence high eigenfrequencies.[20] The main constituents of our setup are a piezo tripod to drive the tip, a mechanical lever system operated by a micrometer screw for the coarse approach of the sample to the tip, and a "stack" for vibrational decoupling. A schematic drawing of the STM is shown in Fig. 1. The body of the microscope is a stainless steel block, which contains the piezo tripod and the screw/lever approach mechanics. The intention of this encapsulated design was to shield the STM from external electric fields and to reduce temperature gradients and hence thermal drift. The operation of the coarse approach is as follows: The L-shaped lever can be rotated around fulcrum II (see Fig. 1), which is realized by a leaf spring. The micrometer screw acts on its long arm, the short arm supports a balance which carries the sample. The balance moves around fulcrum I, which is also a leaf spring. Both springs are mounted under mechanical tension to guarantee firm contact between all parts of the mechanics in each position of the lever. The sample-to-tip approach is achieved by turning the micrometer screw counterclockwise, which causes the long arm of the lever to move to the left and the sample balance to move down. The system operates with high precision and reproducibility, mainly because of the use of springs instead of axes and bearings, avoiding gliding motions to a large extent. The latter would give rise to slipping and, especially under ultra high vacuum (UHV) conditions, friction problems. The sample is mounted on a disk, which for surface preparation and characterization by other techniques can be removed from the STM by use of a wobble stick and transferred to a manipulator in the same UHV system. The thermal stability of the STM is good enough to allow for operation at sample temperatures up to 400 K. *In situ* heating of the sample is performed by radiative heating. The lowest vibrational mode of the piezo tripod is at 7.5 kHz, that of the balance at 2 kHz, which represent reasonably high values. Vibrational decoupling is achieved by a five-story stack of metal plates and viton spacers, which supports the STM in the vacuum chamber, and by supporting the complete UHV system by air sus-

pension mounts. The mechanical stability of the STM with respect to the tip-sample distance is better than 0.01 Å.

Probe tips were made from 0.7 mm polycrystalline tungsten wire by electrochemical etching in a lamella of 2n NaOH in a coil of gold wire (2.5 V dc). They were cleaned in the STM by applying a high voltage to the tip (+300 V) while approaching a gold sheet, until a sudden drop in the field emission current was observed. This treatment resulted in stable but relatively blunt tips. After that treatment a very high resolution state could be obtained during scanning on the aluminum sample, by applying voltage pulses of typically 7 V. This procedure and the resulting change in resolution were described in more detail in an earlier publication.[21]

The STM is part of an UHV system, which is equipped with facilities for LEED and AES, a mass spectrometer, and an ion gun. The base pressure is lower than 1×10^{-10} Torr. During preparation the sample is attached to a manipulator with facilities for cooling and radiative heating. The sample holder was made as small as possible in order to reduce times required for cooling down after annealing. Sample and sample holder were then transferred to the microscope for STM measurements.

The Al(111) crystal was polished with diamond paste down to 1 μm grain size and then electropolished (solution A2 by STRUERS, -4 °C, 38 V, Ni counter electrode). This procedure resulted in an optically flat surface. The subsequent sample treatment in the UHV system consisted of cycles of Ar$^+$ sputtering (3×10^{-5} Torr, 4 μA, 300 K) and heating to 800 K. This procedure was continued until contaminants, mainly carbon and oxygen, were reduced to below the detection limit of AES. The sample then displayed an excellent LEED pattern with sharp spots and low background intensity, indicative of a well ordered surface. STM measurements, however, turned out to be a more sensitive probe for the structural and chemical state of the surface. It required further extensive cleaning cycles before the STM images exhibited a surface characterized by extended, atomically flat terraces of typically several hundred Å width with few contaminations.

Adsorption of oxygen was usually performed with the sample in the STM, at $T = 300$ K. For experiments in the chemisorption regime oxygen pressures in the order of 10^{-7} Torr were used. Most data presented were recorded in-situ, while exposing the surface to oxygen. Shadowing effects, due to the presence of the tip in close proximity to the imaged area, were negligible on the scale of these experiments. Images recorded on surfaces where the sample had been removed from the tip during adsorption yielded identical results.

All STM measurements were performed in the slow scan and constant current mode with tunnel currents between 1 and 100 nA and sample bias voltages typically around -0.1 V. STM data are either shown in a topview grey scale representation with darker colors corresponding to lower levels, or in a quasi-three-dimensional representation, where shading due to illumination from the left is applied. Image processing procedures usually included a planar background subtraction. No filter routines were ap-
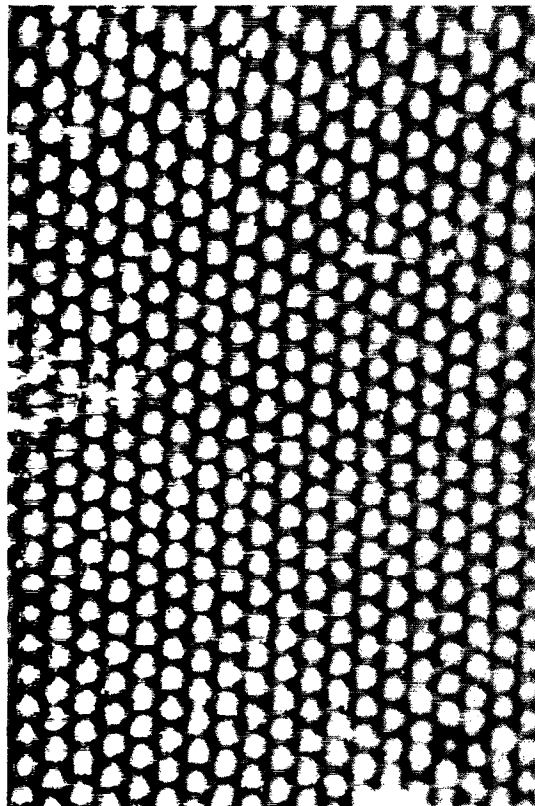
plied. In the case of topview images each terrace was colored by a separate, full grey scale in order to enhance the contrast on the individual terraces. In these images the transition from the grey scale of the upper terrace to that of the lower one causes a black and a white stripe at the step edges.

III. RESULTS

A. The clean and contaminated Al(111) surface

The clean, well prepared Al(111) surface was characterized by extended flat terraces with very few defects. The most prominent type of structural defects observed were monoatomic steps. These showed no preferential orientation but a high concentration of kink sites, in contrast to the tendency to form steps along close packed directions known from high-melting metals such as Ru(0001).[22] Other types of lattice defects such as screw dislocations and point defects were observed only scarcely. On the terraces a hexagonal grid of protrusions could be resolved which reflects the atomic lattice of the clean Al(111) surface. The lattice spacing corresponds to that of the crystallographic distance of 2.86 Å. An example is shown in Fig. 2. These high resolution images were reproducibly obtained for certain tip conditions and for tunnel resistances smaller than typically 10^7 Ω as we have reported in a former paper.[21] At smaller tunnel currents, equivalent to
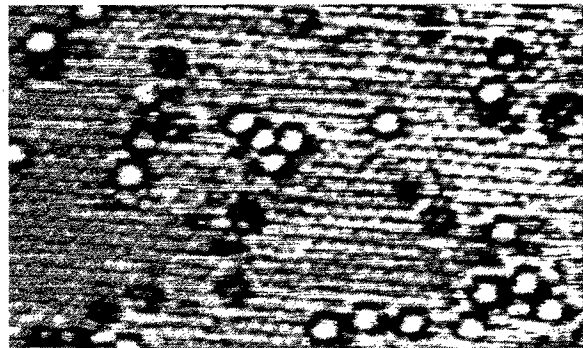

FIG. 3. Typical contaminations of the Al(111) surface after the sample has not been cleaned for several days. White features with dark rings represent carbon atoms ($I_t=9$ nA, $U_t=-0.36$ V, 111 Å×69 Å).

larger tunnel resistances and hence larger gap widths, the measured atomic corrugations decrease rapidly to the detection limit of our STM of about 0.01 Å.

It is still under debate how the anomalously strong atomic corrugations obtained in STM measurements on Al(111) and on various Au surfaces[23] at small gap widths are to be explained. Anyhow, high resolution images such as the one in Fig. 2 demonstrate the high degree of perfection to which the Al(111) surface could be prepared. On this image only a single defect on the lower right corner of the image is detected in an area containing 460 atoms, equivalent to a contamination level of 0.2%. This is in agreement with the information obtained from LEED and AES.

For the surface in a less well prepared state or after longer times (≥ 1 day) between sample preparation and measurement STM images showed a number of foreign atoms on the surface. They are described here because we had to consider the possibility that, even in a low concentration, these "chemical defects" play a role in the adsorption of oxygen. At least two types of additional features can be discriminated in Fig. 3 which were typical for these surfaces. Most remarkable are the bright dots, surrounded by dark rings. In a former paper[24] we have already identified these features as individual carbon atoms adsorbed on hcp sites on the surface. The dark rings reflect adsorbate induced variations in the electronic structure of the neighboring Al atoms rather than topographic effects.[24] For concentrations similar to that present on the surface imaged here (~ 0.02 ML) carbon could already be detected as a small peak in AES.

The second, less abundant type of defects, which can be clearly identified in Fig. 3, are dark ("grey") spots, corresponding to very shallow depressions of ≈ 0.1 Å depth. Closer inspection reveals that these actually comprise three Al atoms which have obviously experienced a change in their electronic structure. Our data favor an interpretation in terms of a subsurface foreign atom underneath the three Al atoms, since the adsorbate itself does not show up in STM images for a wide range of tunnel parameters. Because of the smaller number of these features and the lack of Auger spectroscopic evidence we were
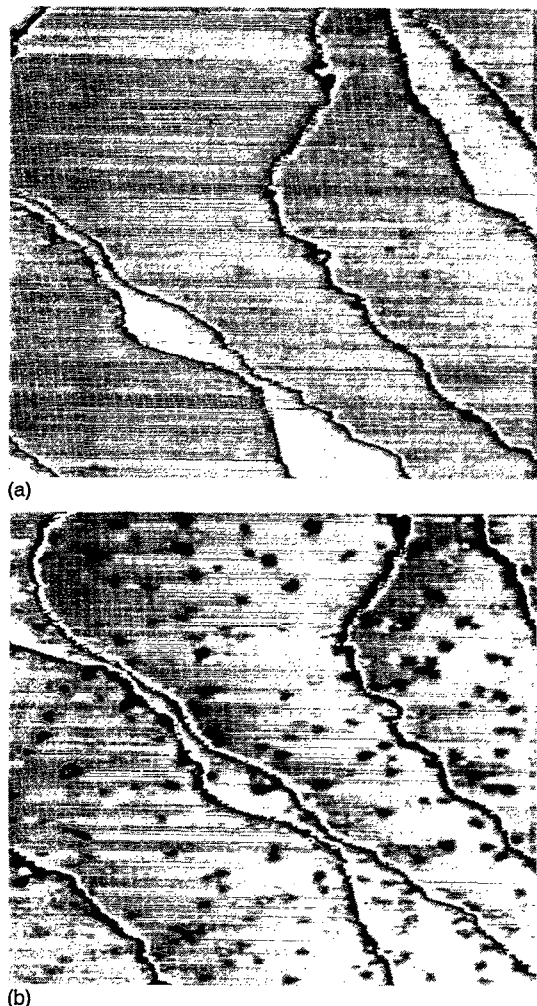
not yet able to specify their chemical identity. A certain number of both features was detected by STM even on well prepared surfaces, in quantities, however, which are mostly below the detection limit of AES.

B. Imaging of adsorbed oxygen by STM

In order to reliably characterize the O adsorption behavior by STM, in particular in the low coverage regime, O_{ad} has to be distinguished from contaminant atoms which might be present on the surface. This is easily possible in the present case, as is demonstrated in STM images which were recorded during adsorption of small amounts of oxygen (Fig. 4). Except for a little thermal drift the area scanned by the STM remained essentially the same during the adsorption experiment. Figure 4(a) shows the surface prior to adsorption, with the typical pattern of irregular steps represented by the black and white lines (see Sec. II). A number of carbon atoms and some of the shallow grey holes, which were described above, can be seen on the terraces. During adsorption of 6 L O_2 black spots appeared
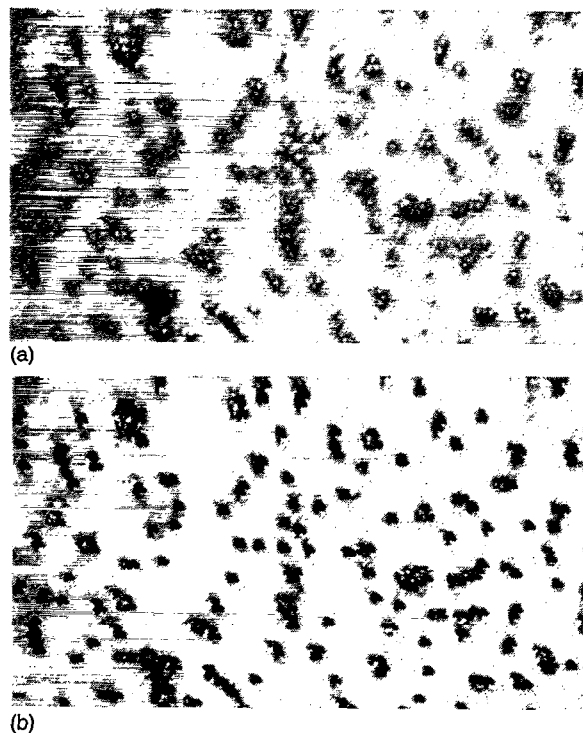
as new features on the terraces [Fig. 4(b)] which are therefore clearly related to adsorbed oxygen. The representation of the adsorbed oxygen by STM is significantly different from that of the carbon atoms and, with an apparent depth of about 0.5 Å, also different from the grey features (0.1 Å depth). It was generally found that for gap resistances $> 10^8$ Ω, mostly corresponding to tunnel currents in the order of 1 nA or below, adsorbed oxygen appears as a depression in the STM images. Depending on the size of the O_{ad} islands and the lateral resolution of the tip, the apparent depth could increase up to 1.8 Å. The data indicate little effect of the bias voltage.

For closer tip–sample distances, i.e., for smaller gap resistances in the order of 10^6 to 10^8 Ω, this situation changes and central protrusions inside the oxygen holes appear. The closest distance of ≈3 Å between neighboring bright "grains" inside the holes in Fig. 5(a) and their orientation along three directions enclosing angles of 120°, both agree well with the (1×1) arrangement predicted for O adatoms. From these observations it is concluded that they in fact represent individual oxygen adatoms. This assignment is confirmed by STM images shown later where larger (1×1) O_{ad} islands are resolved (see Fig. 10). For even smaller gap resistances these protrusions disappear again and instead the O_{ad} islands are imaged as deeper holes, between 1 and 2 Å deep. These effects are illustrated in Fig. 5, which shows a set of STM images recorded after adsorption of 20 L O_2. In these measurements the tunnel current was switched linewise between two values, such
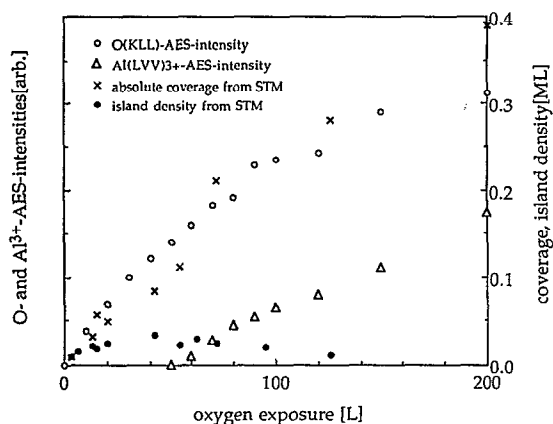
FIG. 6. Auger intensity of the oxygen (KLL) transition ($\bigcirc$) and of the oxidic Al^{3+} (LVV) transition at 54 eV ($\triangle$) as a function of oxygen exposure (E_p=2.0 kV). Oxygen coverage ($\times$) and island density ($\bullet$) as determined by STM (right ordinate) (300 K, $p_{O_2} = 1 \times 10^{-7}$ Torr).

FIG. 7. STM image of Al(111) after 3 L O_2 exposure. Dark features with bright central spots are oxygen atoms (I_t=8 nA, U_t=−0.5 V, 235 Å×227 Å).

that two images of exactly the same area but at different tip–sample distances could be obtained. In image (a) the lines for I_t=28 nA were collected and in (b) those for 70 nA (U_t=−0.1 V in both cases). The bright structure inside the oxygen related holes in Fig. 5(a) (R_t=3.6×10^6 Ω) is not present in Fig. 5(b) (R_t=1.4×10^6 Ω), which was recorded at a closer spacing (Δz=−0.5 Å). The exact value of the gap resistance at which the transformation from the holes at relatively large distances into the more complex structures at higher currents took place, as well as the disappearance of the inner features at even shorter distances, was found to depend on the resolution conditions of the tip. In fact, the latter change could not always be observed.

These effects will be discussed in more detail later. For present purposes it is important to note that for gap resistances around 10^6 Ω the atomic structure of the oxygen features is resolved much better than within the relatively structureless holes obtained for higher gap resistances > 10^8 Ω. Hence, measurements performed with larger tunnel currents provide direct access to the number and arrangement of O adatoms within two-dimensional adatom clusters or larger islands. In particular they allow to discriminate between individual adatoms and agglomerates of adatoms.

C. Adsorption behavior of oxygen in the chemisorption range

The adsorption behavior was characterized by STM measurements, in combination with AES experiments to follow the oxygen uptake. The intensity of the KLL transition of oxygen at 503 eV as a function of exposure is displayed in Fig. 6. This plot covers the chemisorption regime up to 200 L exposure. In this range the oxygen coverage increases steadily with exposure. It is important to note that at exposures below 50 L no oxide is found in the AES spectra, in good agreement with STM observations (see Sec. III D). For the first 35 L the coverage increases almost linearly. The slightly curved shape of the
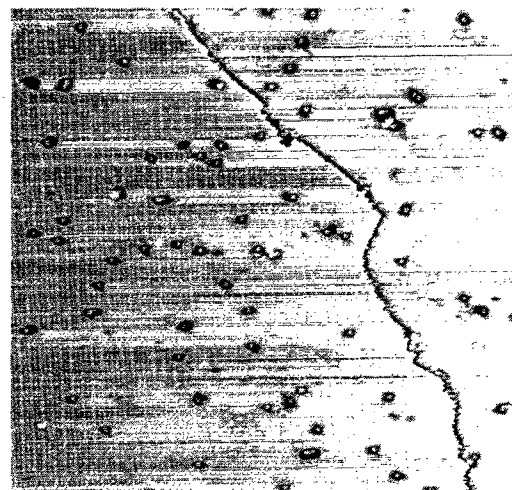
uptake curve corresponds to a continuously decreasing sticking coefficient, in good agreement with results from the literature.[6,8,25] The relative coverage scale of these AES measurements was calibrated by comparison with high resolution STM images, which allowed a direct coverage determination by simply counting the O adatoms. The STM coverage-exposure data are marked as crosses in Fig. 6, with the coverage scale given at the right-hand side of that figure. The scale for the AES intensities is adjusted in such a way as to give a best fit to the STM data, i.e., the AES intensities can be directly converted into absolute coverages. The agreement between AES and STM based uptake curves confirm the representative character of the latter data. Based on these STM data the initial sticking coefficient at 300 K is determined to s_0=0.005±0.0005. It drops with increasing coverage.

Further information on the actual adsorption process was extracted from the coverage and time dependent distribution of O adatoms on the surface. The image in Fig. 4(b), recorded after an exposure of 6 L, points to a random distribution of the adsorbate over several terraces. In particular surface steps do not act as preferential adsorption sites. A more detailed evaluation of those images, however, is complicated by the lack of atomic resolution for the adlayer, i.e., we do not know whether the minima in Fig. 4 correspond to individual adatoms or to small clusters of adatoms. This question is resolved by the high resolution image in Fig. 7, which was recorded after 3 L O_2 exposure under such tunneling conditions that individual O adatoms could be identified by their central protrusion. In addition to oxygen adatoms this image also displays some carbon atoms and a few of the grey features, both of which are easily discerned from O_{ad} by their characteristic appearance in the STM image. Furthermore, it demonstrates that the location of the O adatoms is not correlated with the other foreign atoms, i.e., there is neither an accumulation nor a depletion zone of oxygen around these contaminants.

Oxygen atoms can adsorb in the direct vicinity of these defects, but are not preferentially found at these locations. In images which were recorded subsequently on the same area, no changes in the locations of oxygen atoms were observed, indicating a very low mobility of the (equilibrated) O adatoms on Al(111) at room temperature. [The somewhat "fringed" appearance of the step edges in Figs. 4 and 7 is a dynamic effect, i.e., Al step atoms are displaced between two scan lines with a certain probability. This indicates mobility of step atoms, most likely along the step edges. Steps with many kinks exhibit a higher mobility (lower part of Fig. 7) than straight [1$\bar{1}$0] oriented steps (upper part in Fig. 7).] By counting the protrusions in the STM image, an absolute oxygen coverage of 0.009 ML can be determined for this surface. Evidently, for such low coverages there exist almost exclusively single oxygen atoms and only very few pairs, with atoms on neighboring adsorption sites ($d \approx 3$ Å).

The observation of individual and at the same time immobile adatoms is of course in contrast to expectations based on a naive picture of dissociative O_2 adsorption, where the O_{ad} would be expected to exist in pairs of neighboring adatoms. At least there should be a close spatial correlation between atom pairs. STM images from surfaces with very low oxygen coverages as those presented in Figs. 8(a) and 8(b), recorded after exposures of 1.1 and 2.1 L, respectively, do not show any indication for such a correlation. (Although the individual adatoms are not resolved in these images, we can, based on the results in Fig. 7, safely interpret the minima as representing individual O adatoms.) For a more quantitative analysis we evaluated the adatom densities around given oxygen atoms in these images as a function of distance from those atoms. The density was calculated by counting the adatoms in an annulus of a certain width around the center adatom and dividing this by the area of that annulus. This procedure was repeated for increasing distances yielding the distance dependent adatom density around a single given adatom. For normalization the average of these functions over all adatoms was finally divided by the adatom density of the complete image. The density distribution obtained for the image in Fig. 8(a) is plotted in the histogram in Fig. 9 (the width of the annuli used was 40 Å). We find that the data scatter only little around 1, as it would be expected for oxygen atoms which are randomly distributed over the surface. If there were a pair correlation between the oxygen adatoms this should show up in marked deviations of that function from unity. In addition, the total coverages of 0.0014 and 0.0029 ML in the two images were used to calculate mean separations between neighboring adatoms. We find this to be 80 Å in Fig. 8(a) and 56 Å in Fig. 8(b). Similar results were obtained also for lower coverages around 3.7×10^{-4} ML, where the average distance between oxygen adatoms is about 130 Å. Due to the extremely low coverage, however, the statistics are significantly worse than in the above case. From the absence of any pair correlation we postulated the existence of hot adatoms as a short-living, intermediate mobile species,[19] which will be discussed in more detail later.

(a)

(b)
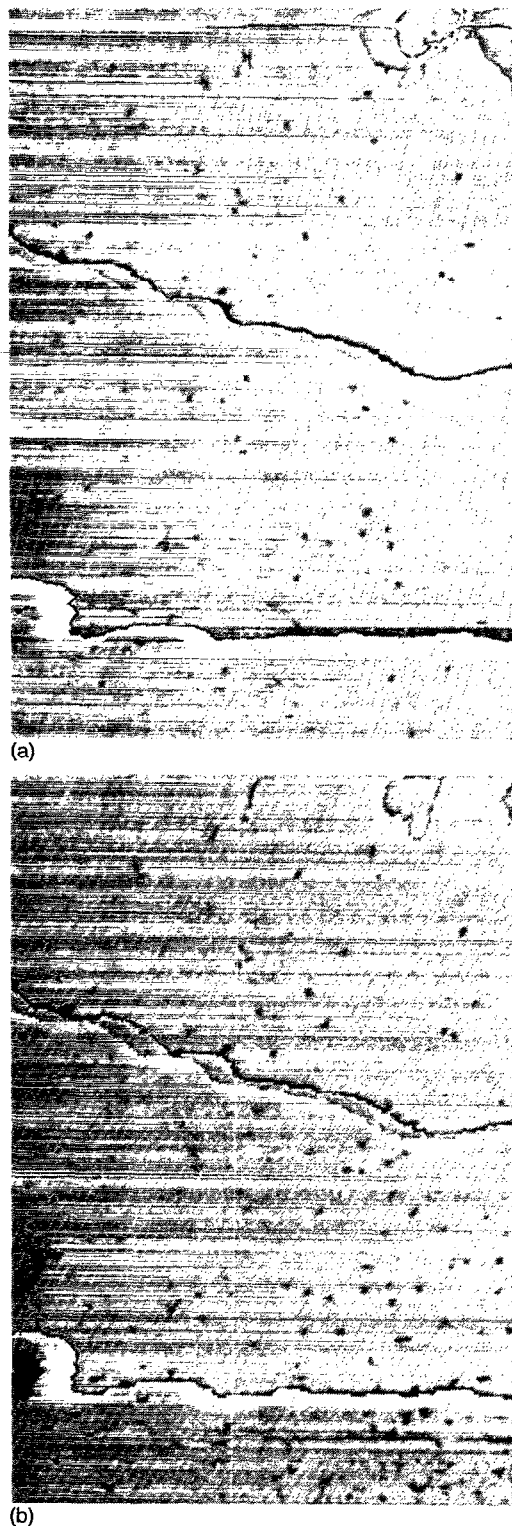
FIG. 8. STM topographs of three terraces of the Al(111) surface, showing individual oxygen adatoms (a) After 1.1 L O_2, $\Theta = 0.0014$ ML; (b) after 2.1 L O_2, $\Theta = 0.0029$ ML ($I_t = 1$ nA, $U_t = -0.2$ V, 474 Å$\times$703 Å).

With increasing coverages more new nuclei are formed, at least up to exposures around 15 to 20 L. This general impression suggested already from inspection of the relatively small area of the O_{ad} covered surface in Fig. 5 (exposure 20 L) is confirmed in larger area images. For

FIG. 9. Histogram showing the relativadatom density vs distance between adatoms in Fig. 8(a).

15 L O_2 exposure we found an island density of $\rho = 0.025$ (number of islands per substrate atom), corresponding to a mean distance of 19 Å between neighboring islands. At this coverage t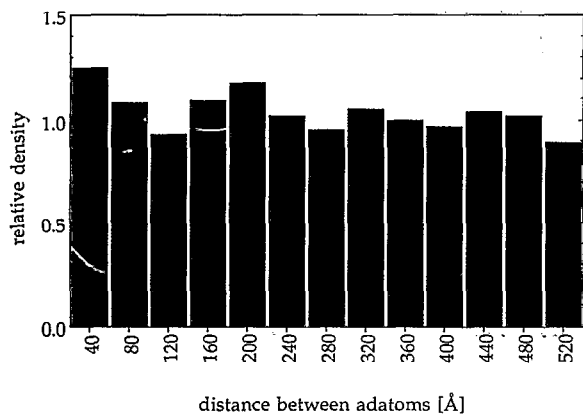he average island size is still small (~ 1.5 oxygen atoms per island, $\Theta \approx 0.038$). Exposure to 20 L leads to the situation shown in Fig. 10. By evaluation of the individually resolved O adatoms the coverage is determined to $\Theta = 0.049$. From the distances between the adatoms in these islands and their orientation with respect to the substrate it is confirmed that local (1×1) structures are formed. (The atomic structure of the metal surface is visible as a weak modulation of the background.) Most striking is the still fairly small size of the islands. The mean island consists of only two O_{ad} atoms, the largest island in Fig. 10 contains 14 atoms. This behavior changes for higher coverages, which is demonstrated in Fig. 11, recorded after exposure to 72 L O_2. Analysis of that image
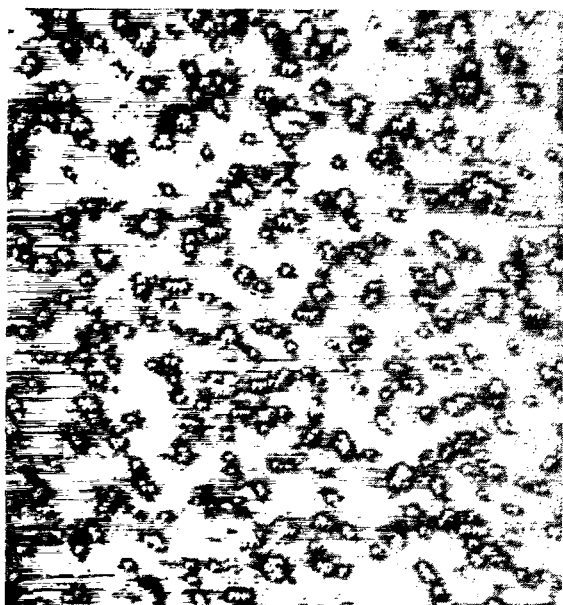

FIG. 11. Al(111) surface after 72 L O_2 exposure with (1×1) oxygen islands. ($I_t = 70$ nA, $U_t = -0.1$ V, 66 Å$\times$73 Å).

reveals an oxygen coverage of $\Theta = 0.21$, with a mean island size of eight atoms. The largest islands consist of about 30 O_{ad}. (The smaller round features at the island edges are artefacts caused by the tip geometry.) The island density of $\rho = 0.026$ ($d_{nn} = 19$ Å), however, has not increased compared to that observed after 20 L. We want to note here that the image in Fig. 11 does not contain any oxide features. Their density is still very small in this coverage regime (see Sec. III D).

The density of O_{ad} islands derived from these and similar STM data not shown here is also plotted in Fig. 6. It increases steadily with coverage, up to exposures around 13 L equivalent to 0.04 ML coverage. The data indicate that below this value adlayer growth proceeds almost exclusively via formation of new nuclei, i.e., via adding individual adatoms. At round 13 L the islands begin to grow on the average while the island density approaches a saturation value of 0.026. Hence further uptake of oxygen occurs exclusively by island growth and no longer by nucleation of new islands. The transition region from pure island nucleation to pure island growth is very narrow. At exposures around 20 L the average island size has already increased to two adatoms per island. For exposures around 100 L the island density starts to decrease again, indicating that at this point the islands start to coalesce. The increase in island size for exposures above ≈ 10 to 15 L is illustrated also by the histogram in Fig. 12, where the island size distributions are summarized for four different exposures, after 3, 13, 20, and 72 L, respectively. Again, there is no significant difference between the distributions found after 3 and 13 L O_2 exposure, although the coverage increased by a factor of 4 in that range. In the low coverage regime, at exposures $\leqslant 10$ L, the adlayer consists almost exclusively of individual adatoms.

Imaging different areas of the surface revealed a ho-

FIG. 10. Al(111) surface after 20 L O_2 exposure, showing small (1×1) O_{ad} islands. ($I_t = 11$ nA, $U_t = -0.1$ V, 242 Å$\times$271 Å).
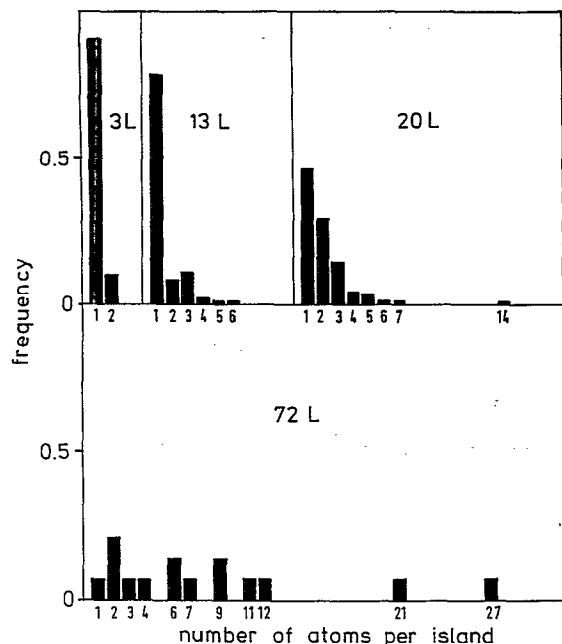
FIG. 12. Histograms showing the size distributions of (1×1) O islands after different exposures, as indicated in the figure.

mogeneous distribution of the adlayer, with no significant differences in coverage or island size distribution. Hence the images can be regarded as representative of the O_{ad} covered surface under these conditions. Also despite of a large number of measurements performed over a wide range of tunneling parameters, we have not detected a second type of chemisorbed oxygen. Our data therefore do not support any models based on coexisting chemisorbed species on different adsorption sites (e.g., surface and subsurface oxygen).

D. Initial stages of oxidation

The presence of a surface oxide on aluminum surfaces is easily detected in Auger spectra by its characteristic peak at 54 eV, caused by a LVV transition of aluminium oxide.[6] A similar peak is observed also for bulk Al_2O_3.[5] In the present study the formation of a surface oxide was followed first by recording the intensity of this peak as a function of oxygen exposure. This is also shown in Fig. 6. (The peak height was obtained by taking the difference of the AES intensity at 54 eV and of the intensity of the clean aluminum spectrum at the same energy, because the LVV transition of metallic Al at 68 eV has some weak satellites on its low energy side.[6]) These data indicate that the oxidation of Al(111) starts at about 60 L exposure, in good agreement with previous studies which reported the onset of oxidation to occur at exposures between 45 and 70 L (55 L,[12,26] 45–70 L,[6] 50 L,[8,25] and 62 L[27]). On the other hand, the STM results presented above for the chemisorption regime demonstrate that for an exposure of 60 L the area covered by the (1×1) O adlayer is only about 13%. Hence the oxidation of Al(111) starts far below the saturation coverage of $\Theta = 1.00$ for an ideal (1×1) layer.

In order to gain more insight into the transformation process from chemisorbed oxygen to surface oxide and in particular to identify possible nucleation and growth phenomena we have performed STM experiments during exposures far into the oxidation regime. In a series of large scale STM images recorded during O_2 exposure up to 1280 L we could follow changes in the surface topography. Except for slight lateral shifts due to thermal drift this series was recorded on the same area, which allows us to directly identify new features that appeared upon prolonged O_2 exposure. Some of these images are shown in Fig. 13, crosses mark identical positions. Before the adsorption experiment the surface area imaged here exhibited the typical step terrace topography with the irregular terrace shapes and terrace widths up to a few hundred Å [see image in Fig. 13(a), recorded after exposure to 2.4 L O_2]. After 100 L O_2 exposure [Fig. 13(b)] the terraces display a characteristic, granular pattern of fine, dark spots (see inset). Under the applied tunnel parameters chemisorbed oxygen atoms are imaged as holes, and the dark spots are thereby identified as O_{ad} islands. These are homogeneously distributed over the terraces without any obvious density variations along the step edges. Examining the image more closely we also find a few, bright features. After 280 L [Fig. 13(c)] the terraces appear even rougher and now these protrusions are clearly visible. Their height is about 1 Å, and their lateral dimensions are slightly larger than the sizes of the O_{ad} islands. Since they appear first in the exposure range where, according to AES, surface oxidations sets in, we associate them with nuclei of aluminum oxide. In this initial stage of oxide formation more of the oxide grains are found at the upper edges of steps than on the flat terraces, indicating a slight preference for nucleation at step edges.

In later stages of the oxidation the number of oxide grains on the flat terraces increases slowly, which is demonstrated in Fig. 13(d), recorded after an exposure of 790 L. These additional grains are randomly distributed over the terraces. In contrast to the density increase the size of these grains has hardly changed, neither laterally nor in the apparent height, which is still less than that of steps. Hence oxide formation proceeds exclusively by the formation of new oxide grains with a characteristic, constant size of about 10–20 Å in diameter rather than by growth of these grains. After 1280 L (not shown here) the remaining parts of the flat terraces do not exhibit any more the granular pattern in higher contrast displays. This indicates that at that exposure the bare surface areas have been completely covered by chemisorbed oxygen, i.e., the O adlayer is practically completed to a total coverage close to 1 ML. A further important result of this series is the observation that the step-terrace topography defined by the position and shape of steps has not changed throughout the adsorption/oxidation process. Also no islands or holes in the topmost Al layer are created. Since steps are the most likely sources or sinks for (diffusing) metal adatoms modifications in the step shape might be expected for a reaction where the density of surface metal atoms is changed with respect to that of a clean metal surface. While the Al sur-
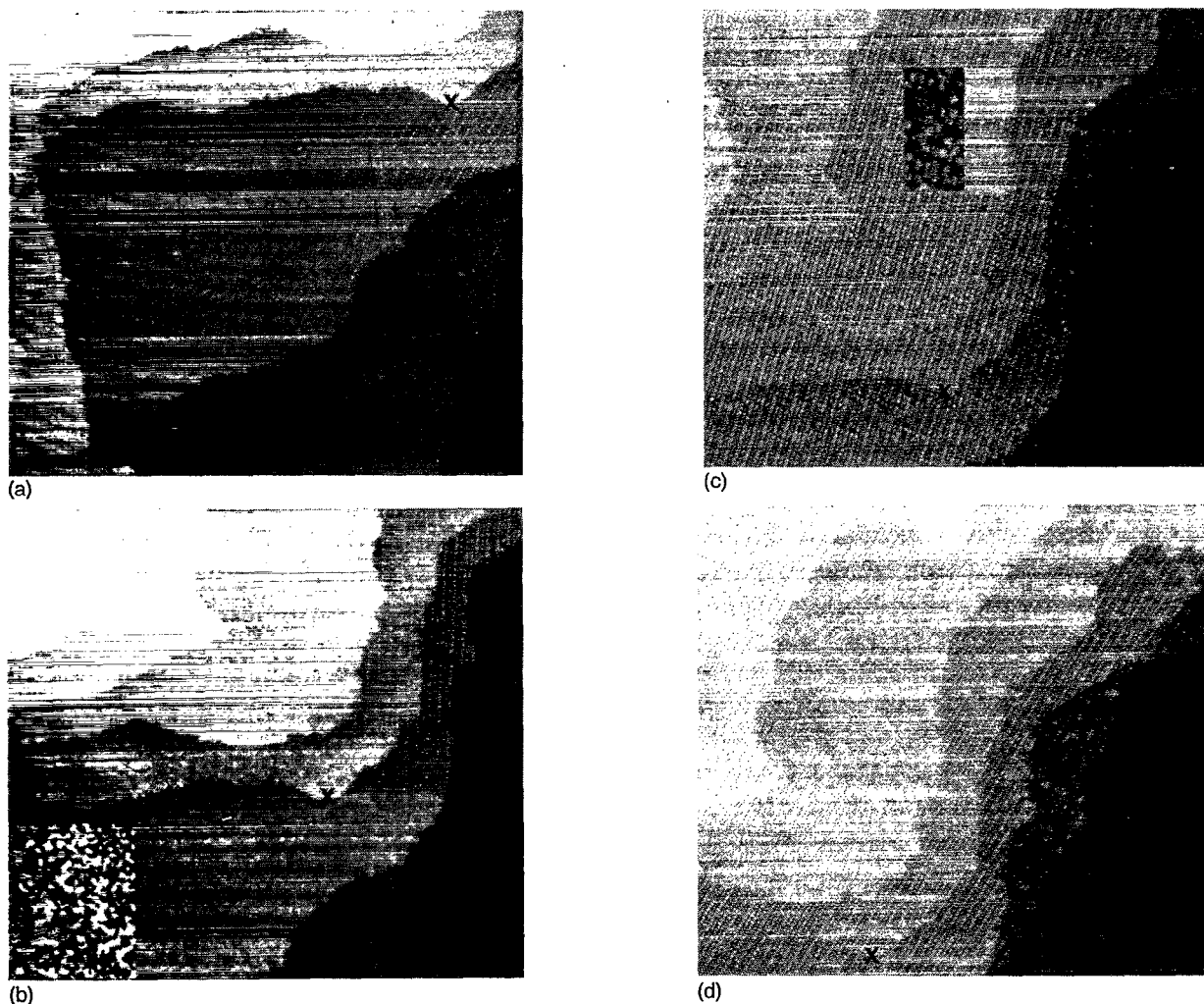
FIG. 13. Series of large scale images ($660 \text{ Å} \times 580 \text{ Å}$) recorded on the same area during oxygen adsorption up to the oxidation range: (a) (almost) clean surface (2.4 L), (b) after 100 L, (c) 280 L, and (d) 790 L O_2 exposure ($p_{O_2} = 2 \times 10^{-8}$ Torr up to 1×10^{-6} Torr, $I_t = 0.1$ nA, $U_t = -1$ V).

face layer density remains constant during chemisorption, it certainly changes at least on a local scale during oxide formation, since the Al density in aluminum oxide (47 atoms/nm^3 for α-Al$_2$O$_3$ and 42–47 atoms/nm^3 for γ-Al$_2$O$_3$) is different from that in metallic aluminum (60 atoms/nm^3). This change in density has to occur and to be accommodated on a rather local scale. Any long range transport of Al atoms can be ruled out for this reaction at 300 K from our images.

These conclusions hold true also to much higher coverages. Even after exposure to 5×10^5 L, the highest dose investigated in this study, there is no qualitative change in the oxidation behavior. As shown in the image in Fig. 14 the terraces are now completely covered with a layer of oxide grains. There are still no features larger than 30 Å in diameter and the average grain size is still of the order of 10 to 20 Å. Most remarkably, the flat terraces and step edges are still visible. Even up to these exposures the oxidation process does not alter the overall topography of the surface, underlining the distinctly local nature of the surface reaction. As a result, for oxidation at 300 K a homogeneous layer of aluminum oxide grains is obtained, with no long range order over distances exceeding 10 to 20 Å.
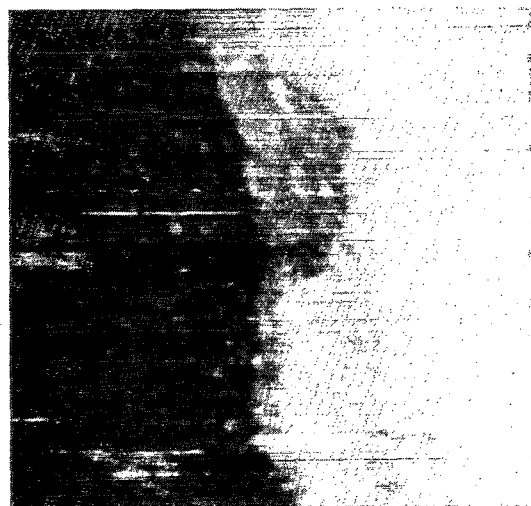

FIG. 14. STM image ($700 \text{ Å} \times 700 \text{ Å}$) of a highly oxidized surface after exposure to 5×10^5 L O_2. The surface exhibits a granular structure caused by small oxide grains. Nevertheless steps and terraces of the former metal surface are still clearly visible ($I_t = 1.0$ nA, $U_t = -0.5$ V).
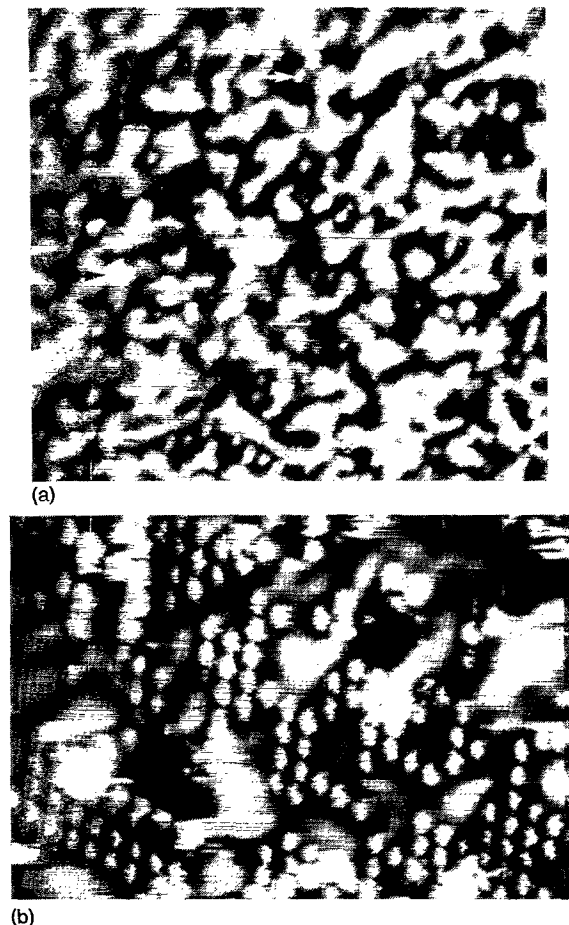
FIG. 15. Small scale STM images recorded in the initial stages of oxide formation, after 126 L (a) and 340 L (b) O_2 exposure. First oxide nuclei are resolved as white protruding grains (arrow). Only part of the surface is covered by chemisorbed O_{ad}, while on other parts patches of bare Al exist; O_{ad} covered areas are imaged as depressions (dark) of ≈ 0.9 Å depth below the bare Al surface level. O adatoms in the (1×1) O islands are resolved in (b). (a): 145 Å $\times$ 140 Å, (b) 58 Å $\times$ 42 Å; $U_t = -0.5$ V, $I_t = 10$ nA).

There might be a short range order within the oxide grains, which, however, was not resolved in the present study.

Further information on the structural and mechanistic aspects of the oxidation process is obtained from smaller scale, high resolution images recorded in the initial stages of oxidation (Fig. 15). After 126 L O_2 exposure irregular grey and dark patches cover the image. Again the deeper, dark areas represent O_{ad} islands, while the higher lying grey areas are bare aluminum regions. Evidently for this exposure the oxygen islands start to coalesce, while still about 60% of the surface is uncovered. Hence the surface is still dominated by patches of the bare aluminum surface. (The O_{ad} islands are very irregular, reminiscent of dendritic structures. Nevertheless a preferential orientation of the island edges along the three symmetrically equivalent lattice directions is visible). In addition to the bare metal and O_{ad} covered areas we find a number of bright protrusions, which, based on the previous arguments, represent oxide nuclei. Most of these features appear as small round protrusions of 0.8 to 1.2 Å height above the substrate level. Since the smallest of them (see arrow at the top of the

image) are only 4 Å in diameter, they cannot consist of more than a few aluminum and oxygen atoms. In addition, Fig. 15(a) shows a few larger oxide clusters with a diameter of about 10 Å (see arrow at the left). Both, the larger and the smaller oxide clusters are located at the borders between O_{ad} islands and the bare aluminum surface. This has implications for the mechanism by which oxygen islands are transformed into aluminum oxide. The adlayer structure resolved here is directly comparable to that observed in the larger scale images shown before. The larger oxide clusters are identical to the oxide grains observed in those images. The small, isotropic oxide nuclei found in Fig. 15(a), however, could not be resolved in the previous images.

In Fig. 15(b) it is seen that even after 340 L O_2 exposure, i.e., long after the onset of the oxidation, well ordered (1×1) O adlayer islands are still present and that a considerable fraction of the surface is still uncovered.

In summary, there is a slight preference for heterogeneous oxide nucleation at step edges in the early stages. With increasing exposures oxide formation is observed also on the flat terraces, mainly at the interfaces between bare surface and O_{ad} covered areas. These oxide nuclei are very small, about 4 Å in diameter. At 300 K they grow up to 10–20 Å. Further oxidation proceeds via formation of additional oxide nuclei. Most important, oxidation starts already when large parts of the surface are still present as bare metal, while the remaining part is covered by a (1×1) O adlayer. On the other hand, there is already a significant amount of surface oxide formed when at ~ 1300 L the (1×1) O adlayer is completed and no bare surface areas are found any more. Finally, at 5×10^5 L O_2 the entire surface is covered by a layer of small oxide grains of 10 to 20 Å diameter. The overall step-terrace topography of the surface is maintained throughout the reaction range and neither island nor hole formation is observed. This rules out any appreciable long-range transport of Al atoms during surface oxidation at 300 K and points to a strictly local mechanism for this process.

IV. DISCUSSION

The STM results presented in the preceding chapter give new insight into the interaction of oxygen with Al(111). In combination with published data they provide a consistent and relatively simple description of the adsorption/oxidation process, which shall be derived in the following chapter. At first, however, we want to discuss a problem related with the applied technique, namely the imaging of adsorbed oxygen atoms on Al(111) by STM.

A. Imaging of adsorbed oxygen atoms with the STM

Under "usual" tunneling conditions, i.e., for tip–sample distances corresponding to gap resistances of the order of 10^8 Ω or more, adsorbed oxygen atoms were found to be imaged as depressions. These were typically between 0.2 and 0.6 Å deep, depending on the exact tunneling conditions. For larger O_{ad} islands holes as deep as 1.8 Å were observed. Of course, this observation does not allow to directly determine the exact adsorption geometry, in par-

ticular the vertical position of the oxygen atoms with respect to the topmost aluminum atoms. The latter question, whether oxygen atoms on Al(111) reside on top of the Al surface atom layer (surface oxygen) or below that (subsurface position), has been discussed controversially in the past.[7] STM does not provide a straightforward answer to this problem, since images of adsorbed foreign atoms reflect the change in the local electronic structure imposed by the presence of the adsorbate, i.e., they represent mixtures of the geometry and the electronic structure of the respective adsorption complexes.[28] The adsorption geometry can, at least in principle, be extracted indirectly from the STM image, if the effect of the adsorbate on the LDOS at E_F is known for different adsorption sites. In fact first calculations on STM imaging of adsorbed oxygen atoms exist,[29–31] which are applicable to the present system and which allow a more detailed discussion. Lang[29] treated the metal surface in the jellium model (with $r_s = 2$ bohr for the electron density, roughly equal to 2.07 bohr for Al) and calculated variations in the electronic state density which are induced by the presence of an adsorbed oxygen atom. For the adsorption site a position above the first layer of metal atoms was assumed. It was found that in accordance with expectations from the high electronegativity of oxygen charge is shifted from the metal to the oxygen atom. Energetically, however, this additional electron density is essentially concentrated in the $O(2p)$ states, which are located about 7 eV below E_F. It does therefore not contribute to the tunnel current in the STM, which probes density of states directly at E_F. At E_F, on the contrary, the calculations revealed a net decrease of state density with respect to the clean metal due to the redistribution of charge, i.e., this charge is repelled by the negatively charged O_{ad} in front of the surface. This led to the prediction of a negative tip displacement above the adsorbed O atom,[29] in agreement with the experimental finding for not too small tip–sample separations ($R_t > 10^8\ \Omega$). (The experimentally observed depth, however, was larger than 0.1 Å, the value obtained in the calculations.) Under these conditions, where the overlap of the wave functions of the two electrodes is small, STM essentially probes the contours of LDOS at E_F in agreement with the general perception. Furthermore, as the calculated state density is almost flat down to about 3 eV below E_F, only minor effects of the bias voltage on the images are expected, also in accordance with the experimental observation.

On the other hand, the calculated decrease in the state density at E_F cannot account for the appearance of the additional structure inside the oxygen holes, which was observed in the experiments for small tip–sample distances ($R_t = 10^6$–$10^8\ \Omega$). These deviations in the STM traces from the contour lines of the LDOS at E_F are believed to result from the simplifying assumptions made in first model calculations of the tunnel current[32] where only spherically symmetric wave functions were allowed for modeling the tip and where the validity of the Bardeen formula was implied. The calculations for O/Al(111) and O/Ni(100) by Doyen and co-workers included both a more elaborate description of the tip and a calculational scheme allowing

for tip–sample interactions.[30,31] Although they did not reproduce the experimentally observed minimum at medium and larger tunnel distances, they found a pronounced variation in the tunnel contours with varying distance in the case of oxygen on Ni(100).[30] These effects were explained in terms of an overlap of the inner, oscillatory parts of the wave functions, which contribute strongly to the tunnel current for very short distances. This can give rise to interference effects between the wave functions and may lead to the deviations of the tunnel trace from the LDOS contours at small separations observed in our case. At larger distances, in contrast, the tunnel current is dominated by the overlap of the exponentially decaying tails of the wave functions and largely follows the LDOS contour lines.

Former experimental studies of oxygen on other metal surfaces all revealed depressions in the STM contours above the O adatoms,[28] similar in character and depth to those reported here for Al(111) at usual tunnel conditions. As with those systems oxygen is known to be located at sites above the topmost metal layer, the present finding is compatible with a position of the O_{ad} *on* the Al(111) surface, but a subsurface site cannot be ruled out solely on the basis of the representation of adsorbed oxygen in STM images.

B. Oxygen uptake and sticking coefficient in the chemisorption regime

The correct determination of the oxygen uptake and the sticking coefficient in this system has long been hampered by the lack of a simple internal standard for the absolute coverage calibration, such as the formation of an ordered adlayer with a structure different from that of the substrate. For O/Al(111) a (1×1) adlayer structure of chemisorbed oxygen was generally accepted, but there was no agreement on when this was saturated. So far two different methods have been employed. The first one relied on the shape of the uptake curves, as they were obtained, e.g., by recording the intensity of the $O(1s)$ state in XPS[8] or of the $O(KLL)$ transition in AES.[6,12,25,26] These curves, which closely resemble our own oxygen AES data shown in Fig. 6, show a steadily decreasing adsorption rate, until at exposures between 200 and 250 L they appear to be saturated. This coverage was then assumed to coincide with the saturation of the (1×1) adlayer, i.e., to $\Theta_O = 1$.[25] Alternatively it had been assumed that the onset of oxide formation between 50 and 100 L signaled the completion of the (1×1) oxygen layer, thus providing a smaller exposure for the $\Theta_O = 1$ calibration point.[12,26] As already mentioned above, we observed the 54 eV peak in AES, which indicates oxidation, to emerge at 60 L, within the exposure range reported in former publications. The STM images resolving individual O adatoms provide a unique opportunity for an exact, absolute coverage determination. They can be used to calibrate the relative coverage scale of uptake curves obtained from spectroscopic measurements, as was done in Fig. 6. The pressure calibration as a potential source of deviations on the exposure axis appeared to be comparable to other studies, since similar exposures were required for saturation of the *oxygen AES peak and for the*

onset of oxidation. From our data it is clear that both methods used for coverage calibration previously lead to far too high coverage values. Correspondingly, the coverages given in earlier studies are generally too high. On the one hand, at the onset of oxide formation around 60 L the chemisorbed oxygen layer is far from being complete $[\Theta(O_{ad}) \approx 0.13$ ML], and on the other hand, a significant amount of oxide has been formed and is already present on the surface at the apparent saturation coverage observed by AES around 250 L where $\Theta (O_{ad})$ is still only 0.4 ML. In fact, there is no saturation even for very high exposures. In the high exposure range exceeding a few hundred L further oxygen uptake is very slow, but still noticeable also in AES measurements. During room temperature adsorption we found the O(KLL) intensity to slowly increase at least up to exposures around 10^4 L. In addition, also the limited probing depth of the AES measurement contributes to the impression of a saturation around 200 to 300 L. Accordingly, comparative measurements of the O(KLL) AES signal and the O(1s) intensity in XPS revealed a significantly higher saturation exposure in the latter case, as expected from the larger escape depth of the O(1s) electrons.[8] Recently an absolute coverage of 0.3 ML was estimated after room temperature exposure to 100 L O_2, based on the total intensity of the O(1s) peak in XPS.[17,18] This is close to the value determined from our data, Θ (100 L) = 0.24 ML.

For the initial sticking coefficient a value of $s_0 = 0.005$ is derived from our data, which is lower than those published so far ($s_0 = 0.02$, 0.03, and 0.04 were reported in Refs. 8, 6, and 25). To a large extent the differences are caused by the differences in the absolute coverage scale as mentioned above. In view of the very high adsorption energy of oxygen on Al surfaces[7] an initial sticking probability of 0.005 appears to be very small, pointing to a considerable activation energy for dissociation. This may be associated with the absence of d electrons in Al, which for transition metals are known to reduce the barrier for dissociative adsorption processes.[33] On the other hand, it was found in HREELS experiments[34] that even at 30 K oxygen still adsorbs dissociatively, with an even higher sticking coefficient than at 300 K. This may even indicate a negative activation energy for the overall adsorption process, and the participation of a weakly held molecular precursor in the adsorption. The small sticking coefficient could then result from possible geometric restrictions of the activated complex, i.e., from an entropy effect as has been discussed for the dissociation of N_2 on Fe(111).[35] Unfortunately the present situation is less clear since at 120 K the sticking coefficient was found to be lower than at both 300 and 30 K.[34]

Our data do not show any correlation between the distribution of oxygen atoms and steps or foreign atoms, in particular there was no agglomeration of oxygen atoms in the vicinity of these defects. However, all we can conclude from this observation is that oxygen atoms are not effectively trapped on these sites (see Sec. IV B). A higher dissociation efficiency at defects cannot be ruled out from our results. Hence, the result of a comparative study on smooth and stepped Al(111) surfaces, which indicated a

significantly more rapid oxygen uptake on the latter surface by about a factor of 4 as compared to the smooth surface,[36] does not contradict our results.

The general shape of the uptake curve in Fig. 6 is comparable to those reported in the literature.[6,8,25] Distinct breaks in the slope of the uptake curve, as they had been reported in Refs. 12 and 26, could neither be reproduced in other studies nor in our measurements. A layer-by-layer growth of the adsorbed/incorporated oxygen, as it was put forward by the authors of Ref. 12 to explain the observed breaks at 50 and 200 L, can also be ruled out from our STM observations.

C. STM results on the mechanism of dissociative adsorption and adlayer formation

Although STM is a static method on the time scale of atomic processes, the observations presented above allow conclusions on the dynamics of the adsorption process, on mechanistic details of the dissociation of the adsorbing oxygen molecules and on the formation of (1×1) O_{ad} islands. These conclusions are deduced from the spatial distribution of oxygen atoms on the aluminum surface at very low coverages (Figs. 7 and 8) and from the coverage dependent size distribution of (1×1) O_{ad} islands (Figs. 6 and 12). The data show that at low coverages in the range up to 3% of a monolayer only isolated oxygen adatoms are present on the surface. There is no immediate formation of islands, in contrast to the usual behavior of oxygen adsorbed on transition metal surfaces.[1] Since island formation does occur at higher coverages (or higher temperatures), this must be caused by kinetic restrictions. The mobility of the O adatoms, thermally equilibrated on the Al(111) surface, is very low at 300 K, which prevents the formation of islands for small coverages. In fact, atomic resolution images, which were recorded consecutively on the same surface area, did not show any displacements of oxygen atoms onto neighboring sites. From this observation an upper limit for the surface diffusion constant of oxygen adatoms on a Al(111) surface can be calculated. The area of Fig. 7, which contains 42 O adatoms, was imaged 120 s later and no O_{ad} displacement was found. Therefore the root mean square displacement must be smaller than 0.22 Å in 120 s. This corresponds to a surface diffusion coefficient $D < 4 \times 10^{-20}$ cm^2 s^{-1}, equivalent to a minimum activation barrier for surface diffusion of about 1.0 eV, if we assume $D_0 = 5 \times 10^{-3}$ cm^2 s^{-1} for the preexponential factor. This is a rather high value for a surface diffusion barrier, but it does not contradict expectations for a strongly chemisorbed surface atom such as oxygen on Al(111). (The adsorption energy of oxygen on this surface is experimentally not accessible, but for the binding energy values as high as 12.3 eV were obtained in calculations[37]). A very low, though measurable mobility has been observed by STM for oxygen atoms adsorbed on Ni(100) at 300 K.[38]

The STM images recorded at very low coverages show that the first oxygen atoms are randomly distributed on the surface. These two findings, of immobile oxygen atoms on the one hand and of their random distribution on the other

side, are in apparent contradiction to naive expectations for a dissociative adsorption process, which would predict spatially correlated pairs of atoms. This problem is resolved by the assumption of a short living mobile atomic species, which precedes the final, immobile adsorption state. These hot adatoms result from an internal energy transfer during dissociative adsorption.[19,39] Part of the energy released during this process is transformed into kinetic energy parallel to the surface, allowing the two O atoms of a molecule to fly apart by at least 80 Å before their excess energy is dissipated. The value of 80 Å results from the mean separation between two neighboring oxygen atoms at the lowest possible coverage for which we have statistically significant data (Fig. 8). The actual distance traveled by the hot adatoms can be larger than that. This would equally result in a random distribution. We are thus able to put a lower limit on the lifetime of the exited state, based on the following, simplifying assumptions: The total energy gained during dissociative adsorption of the molecule is transformed into kinetic energy of the oxygen atoms, which, because of momentum conservation, fly ballistically into opposite directions parallel to the surface. Furthermore, there shall be a frictional force which decelerates the particles linearly with time. Assuming 6 eV for the binding energy of oxygen atoms on Al(111) (a slightly lower value than that obtained in calculations[7]), and with the dissociation energy of 5 eV for O_2 molecules in the gas phase, an initial kinetic energy of 3.5 eV is obtained for each atom. This corresponds to an initial velocity of 6.5×10^3 m/s. When each of the two atoms comes to rest after traveling a distance of 40 Å, i.e., half the mean distance between two atoms as obtained from the STM images, this would correspond to a lifetime of about 1 ps. This value represents the minimum lifetime of a hot atomic precursor. The lifetime would be larger if the actual distances traveled by the oxygen atoms are larger, if the O atoms travel in a random walk mode or if the adsorption energy is transformed only partially into kinetic energy.

The estimated lower limit for the lifetime of the excited O atoms (~ 1 ps) is of the same order of magnitude as the time constant estimated on the basis of an electronic friction model,[40] but energy transfer via phonon excitation would also be compatible with the lower limit of the lifetimes. Therefore it is not yet possible to decide from the present experimental findings whether the energy release to the solid occurs predominately by multiphonon excitations or by electronic excitations.

It is evident that a ballistic motion of adsorbed oxygen atoms which, once thermalized, are almost immobile, must have implications on the island formation mechanism. The probability for nucleation and growth of islands is significantly reduced by kinetic effects, as compared to the situation of a random walk mechanism for diffusing adparticles, since only a smaller number of adsorption sites is probed. In fact the experimentally observed island growth behavior (see Fig. 6 and the island size histograms in Fig. 12) points to a mechanism which is distinctly different from the usual nucleation and growth scenario. With the strong peaking at single atom islands for low coverages and

with still small islands at the beginning of the oxidation, the distribution is in striking contrast to expectations for an island forming adsorbate. At very low coverages almost exclusively isolated adatoms are present on the surface, and the island density increases linearly with coverage (see Fig. 6). The distribution obtained after 13 L O_2 exposure still looks almost like that determined after 3 L (see Fig. 12), although the coverage increased by about a factor of 4. That is, initially the increase in the amount of adsorbed oxygen on the surface leads almost exclusively to an increase in the number of isolated O_{ad} atoms and very few pairs and triples. Only after a coverage of $\Theta = 0.03$ is reached, the islands begin to grow while the island density saturates (at $\Theta = 0.05$). Hence island growth begins at exposures of 10–15 L, corresponding to coverages of 0.025–0.037 ML, respectively, and saturation is reached at exposures around 20 L (see Fig. 6). These findings will be rationalized in a model where translationally hot adatoms can release their kinetic energy in an inelastic collision with a thermalized adatom or a cluster of adatoms.

This appears plausible from the identical masses of thermalized and hot adatoms providing a very efficient transfer of energy from the impinging atom to the atom at rest. The model explains the finding of exclusively single atom nuclei at very low coverages, since under these conditions the probability for the mobile precursor atoms to find thermalized atoms to which they can attach is very small. It is much more likely that they equilibrate at some position on the bare metal surface. When the coverage becomes larger the chance for the precursor to hit a trapping center on its path increases. Here it will be deexcited with a higher probability than on the bare surface and will attach to the atom already present. For $\Theta > 0.03$ the density of adatoms is sufficiently high so that de-excitation at adatoms and islands becomes more probable and hence the coverage increase leads predominantly to the growth of islands. The distribution of islands as a function of exposure is therefore fully compatible with the concept of hot adatoms. Equal accommodation probabilities on all sites would result in a stochastic site occupation which is clearly different from the experimentally observed distribution.

In order to test this model an attempt was made to quantitatively reproduce the experimentally observed mean island size or, equivalently, the island density as a function of coverage. Based on the above ideas we derived a relation between the island density ρ and the oxygen coverage Θ, which contains the cross-section σ for the inelastic collision of a hot precursor atom with a thermalized adatom or cluster of adatoms and the path length λ of the precursor on the bare surface as adjustable parameters:

$$\frac{d\rho}{d\Theta} = (1-\rho)^{\lambda/A(\sigma\sqrt{(\Theta/\rho)}+\delta)}.$$

Details of the derivation are described in the appendix. For λ we have already derived a minimum value of 40 Å. If we assume the distance between adatoms in (1×1) islands, 2.86 Å, for the cross section σ, we obtain a reasonably good fit to the experimental data for $\lambda = 160$ Å. This is shown in Fig. 16 (lower curve). The experimental data
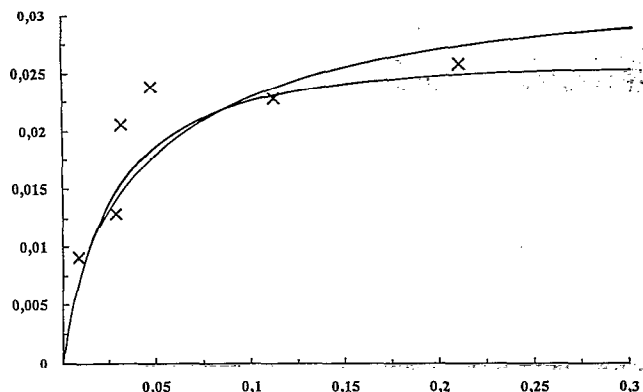
FIG. 16. Fit of the island density vs coverage derived from a model for hot adatom trapping [lower curve: σ (single atom) $= 2.86$ Å, $\lambda = 160$ Å, upper curve: $\sigma = 8.58$ Å, $\lambda = 70$ Å] to the experimental data from Fig. 6 (marked as x).

in the island density vs coverage plot are derived from the data in Fig. 6. Alternatively it can be assumed that the cross-section of a single atom is given by the diameter of the complete adsorption complex, i.e., the adsorbed oxygen atom plus the surrounding metal atoms which are affected by the central oxygen. This quantity can be directly taken from the STM images which revealed diameters of the oxygen holes of about three lattice constants for a single atom. With that number λ becomes 70 Å (upper curve in Fig. 16). Hence, in both cases values for λ are obtained which are somewhat larger than the lower limit of 40 Å obtained above. As a consequence, by assuming reasonable physical parameters the model describes the island growth quite well. We take this as confirmation of the hot adatom concept which also accounts for the island formation mechanism. (During the preparation of this manuscript it was brought to our knowledge that a Monte Carlo simulation of the island growth, which was based on the concept of hot adatoms, revealed excellent agreement with our data[41]).

D. Adsorption geometry of O adatoms and adlayer islands

The structure of the adsorption complex and the adsorption geometry within the islands have for long times been a fundamental problem in studies of the O–Al(111) interaction, leading to a wealth of partly conflicting conclusions. It will be demonstrated that the interpretation depends critically on the knowledge of the actual coverage, i.e., the correct exposure-coverage relation, and on the island size distribution in the coverage range for chemisorption, as they were discussed above.

The plausible idea of a threefold hollow adsorption site above the surface (surface site) brought up first was questioned in later studies based on the observation of an initial decrease of the work function upon oxygen adsorption.[8,9] The decrease was interpreted in terms of oxygen incorporation and hence led to the proposal of a subsurface site, with oxygen atoms between the first and second aluminum layer. Other authors, however, reported either no change

in ϕ up to 30 L (which was thought to correspond to completion of the chemisorption regime)[6,12] or an increase in ϕ,[10,11] in accordance with the usual tendency for surface adsorption of electronegative adsorbates.

Earlier attempts of a direct structure determination could not settle the question of the oxygen position. Neither LEED I/V analyses[42,43] nor SEXAFS measurements[3,4] led to a definite result. The first ones suffered from a too small data set of only two or three beams,[44] the latter ones from the very weak signals for O and Al which allowed only the distance to the nearest Al atoms to be determined. In theoretical studies on O/Al(111), which are reviewed in Ref. 7, also no clear preference for either a surface or a subsurface position was obtained. Only very recently a standing x-ray wavefield adsorption study[15] came up with a clear preference for one adsorption geometry, with O adatoms located in fcc hollow sites 0.7 Å above the Al substrate. That study also supports the view that only a single adsorption site is occupied in the low coverage regime. This result is fully compatible with our STM data, which also provide very strong evidence for a single adsorption site: In none of the measurements could we detect two different kinds of adsorbed oxygen species, throughout the chemisorption range. This leaves us with the problem of rationalizing the complex spectroscopic behavior, in particular the multipeak structure in HREEL spectra, which was reported in a number of earlier studies.[13,14,27,45]

In our opinion the key for the understanding of the experimental data lies in the formation of the extremely small adlayer islands and in the strong interactions between the close packed O adatoms in these islands on the one hand, and in the early formation of aluminum oxide on the other hand. In the (1×1) islands the separation between neighboring O_{ad} is only 2.86 Å. The early onset of oxide growth results in the simultaneous presence of chemisorbed and oxidic oxygen species over a wide range of coverages, between 0.13 and 1.0 ML.

Because of the close proximity of the O adatoms in the (1×1) structure, which is one of the most densely packed oxygen adlayers known for metal surfaces, strong interactions will exist between neighboring oxygen atoms. These manifest themselves, e.g., in the large dispersion of the $O(2p_{x,y})$ band in ARUPS.[10,46–48] (In this context it is interesting to note that the dispersion was observed already at exposures of 4 L, where based on our data only single adatoms exist on the surface. The sizeable total intensity observed under these conditions,[10,46] however, implies that the actual coverage was significantly higher than one would expect from this exposure. Nevertheless, the ARUPS data imply that band structure formation and dispersion phenomena can occur already at extremely small island sizes of a few adsorbed particles only.)

The strong interactions between O adatoms make it likely that adatoms at island edges, because of fewer neighboring oxygen atoms, can be spectroscopically distinguished from the adatoms in the center of these islands. The interpretation of different spectroscopic states in terms of O or Al atoms coordinated to a different number of O
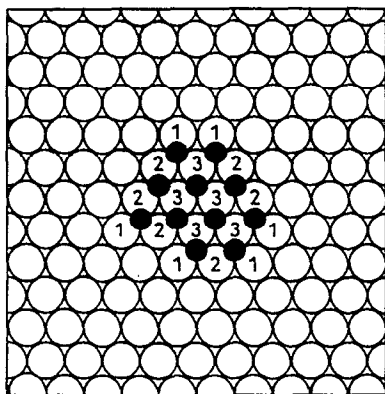
FIG. 17. Typical small (1×1) O_{ad} island on Al(111). Indicated are the numbers of oxygen atoms (full dots) which are directly bound to aluminum atoms (open circles).

adatoms was first proposed by McConville et al.[16] In a photoemission study using synchrotron radiation they resolved additional Al(2p) states in high resolution spectra of a surface covered by chemisorbed oxygen, with binding energies shifted by 0.49, 0.97, and 1.46 eV to higher values with respect to the clean metal state. (The surface oxide is characterized by a wide peak centered at 2.7 eV higher binding energies than the metallic state.) These different values were tentatively attributed to Al atoms bound to one, two, and three O adatoms, respectively. Similar effects with three different adsorbate induced states were reported also for F/Si(111).[49] As shown in the model in Fig. 17 (for which a threefold surface site was assumed), the aluminum atoms at the edge of the island are bound to one or two oxygen atoms, those in the center to three. Because of the small size of the (1×1) islands the number of aluminum atoms in the interior of the islands is comparable to that of Al atoms at island edges over a wide range of coverages, and therefore the edge atoms provide enough intensity to be discernible by spectroscopic techniques throughout the entire chemisorption regime. In contrast, for most other island forming adsorption systems the islands grow rapidly with coverage to sizes so that the edge atoms contribute little to the measured intensity.

The overall development of the island size as a function of coverage corresponds very well to the evolution of the Al(2p) peaks during progressing chemisorption.[16] The three states attributed to aluminum atoms with one, two, and three oxygen attached were found to grow and decrease successively in intensity, as expected in this model. (The slight deviation in the exposure derived coverage scale, as reflected by the onset of oxide formation already at exposures around 10 to 20 L, has no effect on the conclusions drawn from these data.)

Two different O(1s) binding energies of 532.1 and 533.5 eV were observed by Bagus et al.[17,18] in spectra recorded from an O_{ad} covered surface ($\Theta_O \approx 0.3$ ML, exposure 100 L O_2). Since the presence of an oxide phase was ruled out in this work from the absence of any Al^{3+}—AES intensity, both peaks must result from chemisorbed oxygen. By comparison with cluster calculations where they

compared the case of a central O adatom with three or six oxygen perimeter atoms (in a $Al_{19}O_4$ cluster and isolated O_4, O_7 clusters), the higher and the lower energy peaks were attributed to O(1s) states of edge atoms and central atoms in O_{ad} islands, respectively.[17,18] Simultaneous population of surface and subsurface sites could be ruled out as the origin of the double peak: Subsurface oxygen was calculated to have a higher O(1s) binding energy as compared to the surface species. Experimentally, the higher binding energy component was found to increase in relative intensity upon going to grazing emission angles, in contrast to expectations for a subsurface species. The angular behavior was found to be correct, however, if these two peaks were assigned to adatoms at the center or at the perimeter of an island, since a higher O(1s) binding energy had been calculated for the latter species. Both the relative ratios of the two states, indicative of rather small island sizes, and the island growth upon annealing are fully compatible with our data.

Most support for the idea of a subsurface site so far came from the HREELS data, which on the other hand also appear to be most contradictory. The finding of a three peak spectrum already at low exposures (2 L) was taken as evidence that from lowest coverages on both surface and subsurface sites are populated.[13] The two dominating peaks at 80 and 105 meV were assigned to perpendicular stretch modes of surface (80 meV) and subsurface (105 meV) oxygen atoms. This tentative assignment was confirmed by parametrized force constant lattice dynamical calculations, which favored a "double layer" (1×1) structure with O atoms in both surface and subsurface sites.[50] A double-layer structure for the chemisorbed oxygen, in (1×1) islands, was proposed also in a later study, though the peak assignment differed.[34] The smaller peak at 40 meV was attributed to a coupled underlayer-overlayer mode. In later studies[14] the same three peaks were identified. However, both the exposure dependence of their intensity and their assignment differed. Furthermore, a double peak structure was resolved in the central loss at 60 to 80 meV.[14,34]

The interpretation of these data becomes straightforward, if the present STM data are taken into account. There is general agreement that the two loss peaks in the 60 to 80 meV regime, which are present in varying intensity ratios from lowest coverages on, result from chemisorbed oxygen. Based on the STM data and XPS results this double peak structure, which was recently explained by the coexistence of a surface and a subsurface oxygen species,[34] is more plausibly attributed to differently coordinated O adatoms rather than to adatoms on different adsorption sites.

Due to the strong O–O interaction the stretch frequencies of adatoms at island perimeters are expected to be significantly different from those of central adatoms. (Individual adatoms are not considered here because of their low absolute density.) A strong coordination effect in O adlayers vibrations was reported, e.g., for O/Ni(100) where the stretch mode shifted from 53 to 39.5 meV by going from a $p(2\times2)$ to a $c(2\times2)$ adlayer structure, al-

though the adsorption geometry did not change significantly.[51]

From the simultaneous appearance of the low energy peak around 40 meV and the Al^{3+}–AES peak at 54 eV in adsorption and annealing experiments this loss is clearly identified as an oxide specific feature.[27,45] The high energy peak at 105 meV was equally assigned to an oxide specific mode, at least in some of the studies,[27,34] because it was observed only under conditions where oxide was likely to be present. Its strong intensity gain together with the growth of the 40 meV peak points into the same direction. This assignment is apparently contradicted by earlier results,[14] where a multipeak structure containing a loss at 105 meV was reported for extremely low exposures as low as 0.2 L. To our belief this is due to an error in the exposure scale in that study. Much higher coverages than the 0.001 ML calculated from our coverage exposure relation are required to yield loss intensities comparable to the spectra presented there. In that case the data do not contradict the above assignment, which relates the 105 meV loss to an oxide specific mode. The STM data also offer an alternative explanation for the early appearance of the 40/105 meV peaks which caused much of the confusion in the HREELS studies. Our interpretation is simply that this reflects the early formation of aluminum oxide, which we observed at coverages far below the saturation of the chemisorbed layer.

In conclusion, the island structure of the (1×1) O adlayer on Al(111) and the simultaneous growth of chemisorbed layer and oxide offer an alternative explanation for the complexity in spectroscopic data, without the need for an additional chemisorbed subsurface species. Still open is the question of the work function data. However, it has been shown theoretically that even for a surface position of the O_{ad} an unusually small change in ϕ can be expected,[52,53] although there is a large charge transfer to the oxygen. This is a consequence of the very close distance of oxygen to the topmost aluminum layer of 0.6–0.7 Å, as derived from SEXAFS results.[3,4] In that case even the formation of very small amounts of oxide, e.g., at surface defects, might change the sign of the change in work function.

E. Nucleation and growth of surface oxide

Higher oxygen exposures, at room temperature, finally lead to surface oxide formation. The (111) plane is the only Al surface where a distinct chemisorption stage, preceding oxide formation, could be identified. On the other Al faces oxidation begins instantaneously. Our data demonstrate, however, that for Al(111) the situation is rather complex. A pure chemisorption phase is found only at rather low coverages, $\Theta_O < 0.13$. At larger coverages formation of oxide nuclei is observed. Hence oxidation starts already when most of the surface is still bare metal phase. Further oxide formation proceeds parallel with additional oxygen uptake in the chemisorbed phase, and the saturation coverage of the (1×1) phase of $\Theta_O = 1.0$ is reached only when a considerable part of the surface has already been transformed into the oxide state. Over a wide range of

coverages chemisorption and oxide formation occur as competing processes and the rates for these processes are hence of comparable magnitude. This behavior contrasts that found for most metal surfaces, where the oxidation rate is significantly lower than the chemisorption rate, and oxide formation essentially begins only after the chemisorption process is completed, i.e., after the surface is covered by a complete O adlayer.[1]

The finding of a wide coexistence range of three phases, bare metal surface, chemisorbed adlayer and surface oxide, differs from earlier pictures for the O/Al(111) system. This is largely due to the incorrect coverage scale in those studies, where $\Theta_O = 1$ was often assigned to the onset of oxidation. EEL spectra should, at least in principle, allow to follow chemisorption and oxidation independently. In contrast, the total oxygen exposure needed to initiate oxide formation was about the same in most of these studies. Typically values of 50 to 100 L were reported as minimum exposure before oxide formation took place.[7]

In a "nucleation and growth" type description oxide formation on this surface is dominated by nucleation processes rather than by subsequent growth of the oxide nuclei. Oxide nucleation occurs with a rate which is lower by about 1 to 2 orders of magnitude than the adsorption rate (at partial pressures of about 10^{-6} Torr). Subsequent growth, however, is very slow, and oxide grains cease growing, at room temperature, after they have reached a diameter of about 10–20 Å. Oxide nucleation is preferentially observed at the perimeter of O_{ad} islands and bare substrate surface, i.e., it is dominated by a heterogeneous nucleation mechanism. Furthermore there is a slight but significant preference for oxide formation at the upper terrace side of step edges. At medium exposures, 100 to 400 L, these step edges are decorated with oxide grains, while their density on the flat terraces is still rather low. This preference contrasts the chemisorption behavior, where O adatoms and O adislands are homogeneously distributed over the surface with no resolvable preference for step edges.

In a strict sense heterogeneous nucleation is not associated with a critical nucleus size. We know, however, from the STM data that oxide formation begins at coverages where the average island size of chemisorbed oxygen is about 8–9 atoms, and the large islands contain about 20 O adatoms. This may represent a minimum island size (of O_{ad}) for oxide formation.

The above description in terms of a nucleation and growth model does not include information on the actual mechanism of the oxide forming process, i.e. on the atomic scale processes involved herein. The formation of an oxide compound must involve atomic exchange. If we define the oxide as a species where Al–Al bonds are broken and replaced by Al–O–Al bonds, this requires the oxygen atoms to occupy positions between the first and second layer such that Al surface atoms are no more directly bound to second layer Al atoms. Most simply this occurs by oxygen atoms penetrating the topmost layer of the Al lattice. This agrees well with our observation that oxide nucleation is more facile at step edges. Step edge Al atoms are less

tightly bound and hence the oxygen atoms can penetrate more easily the Al lattice at these locations. Correspondingly, on a highly stepped Al(111) surface oxidation was found to start already at much lower exposures, below 10 L.[36] Site exchange and Al lattice penetration by O adatoms as a rate limiting step for oxide formation is also consistent with the different oxidation behavior found on the more open Al(100) and Al(110) surfaces, where oxidation begins right away, whereas on the close packed (111) surface this process is less rapid.

Because of the different densities of Al atoms in the substrate and in Al_2O_3 bulk oxide, oxide formation also requires mass transport of Al atoms. This might occur, e.g., by evaporation of Al atoms from step edges, which can subsequently migrate over the surface. A similar mechanism was recently observed during formation of –Cu–O–Cu– added row strings on Cu(110)[28] and during formation of the $c(6\times2)$ O suboxide phase on the latter surface,[28] which leads to characteristic changes in the step shapes. For Al(111) no such changes are observed during chemisorption or oxide formation. The original step shapes are maintained. In fact the mobility of Al atoms along step edges, reflected by the fuzzy step edges in STM images of the clean surface, is reduced by O adsorption, and step edges appear as continuous lines on the O covered surface. Also on a more local scale there are little modifications in the step terrace topography and the flat terraces of the original substrate can still be recognized after very high exposures, as evidenced in the 5×10^5 L experiment shown in Fig. 14. Hence at 300 K oxide formation takes place on a very local scale with no long range mass transport involved. This is demonstrated also by the small size of the oxide grains (typically 20–30 Å diameter).

Site exchange processes such as oxygen penetration onto subsurface sites are likely to be kinetically limited. The activation barrier can be overcome by thermal activation. For higher O_{ad} coverages close to or slightly above the onset of oxide formation it is in fact well known and also confirmed by our own AES measurements that oxide formation is initiated or enhanced by annealing to temperatures around 500 K. Amazingly, at lower coverages even annealing does not cause any oxide formation, instead the islands of chemisorbed O_{ad} grow in size.[17,18] In conjunction with previous findings, which report efficient oxide formation also at 135 K[27] and even 20 K,[34] this suggests that the normal thermally activated path is not the only possibility for oxide formation. It is suggestive that a mechanism similar to that found already for O chemisorption is possible also for oxide formation, involving the highly energetic hot adatoms. In that reaction scheme oxide formation is initiated by hot adatoms impinging with sufficient kinetic energy on a chemisorbed O_{ad} island. This is consistent also with the observation that oxide nucleation occurs at the perimeter of the O_{ad} islands. Though we cannot provide direct evidence for such a reaction mechanism, the combined experimental evidence makes it very likely. In this reaction scheme the immobility of the O adatoms and small adislands at 300 K also play an important role for the early onset of oxidation. They allow an efficient energy

transfer from the hot adatoms to the Al–O structure of the existing islands.

The oxide grains have never been observed to dissolve again at 300 K, indicating a high stability of the oxide phase. This of course agrees well with the very high heat of formation for aluminum oxide (17 eV for α-Al_2O_3).

In the course of this work we never resolved atomic structures in the oxide grains. Their often irregular shapes as well as their small sizes are consistent with the results of LEED investigations, where the general decrease in Al(111) spot intensity in a rising background, with no new spots emerging, led to the conclusion of an amorphous adlayer.[7,54] It should be noted that this does not require the individual grains to be amorphous as well. Small crystallites with random orientation are also compatible with the data. Regardless of these two possibilities it is clear that there is no epitaxial oxide growth at room temperature. Only upon annealing to or reaction at elevated temperatures an epitaxial crystalline oxide layer can be produced.[54]

Altogether oxide formation on Al(111) resembles that found in a recent STM study on O/Ni(100) and that for suboxide formation on Cu(110) in many aspects, pointing to a more general validity of these results for metal oxidation processes. Also on Ni(100) oxide formation occurs preferentially at step edges, while there is no preference for oxygen chemisorption on these sites. This tendency is even more pronounced at slightly higher temperatures. Preferential nucleation at step edges of course is very plausible since in all of these cases site exchange is required for oxide formation.

On the other side, distinct differences also underline the chemical and structural effects of the respective surfaces. The pronounced coexistence range of the three phases—oxide, chemisorbed oxygen and bare metal surface, for instance was not found with O/Ni(100). In that case oxide formation starts only after the surface is completely covered by chemisorbed oxygen. The late onset of oxidation, often preceded by an 'induction' period, in fact seems to be typical for metal surface oxidation.[1] A second noticeable difference between the two systems is observed in the subsequent stages of oxide formation, which on Ni(100) proceeds, at least to a good deal, by lateral growth of the nuclei at step edges, while on Al(111) additional nuclei are formed on the flat terraces. For a more general discussion of the microscopic aspects of metal surface oxidation, however, the data base is too small so far, and further studies of this type are required for a better understanding of the oxidation process.

V. CONCLUSIONS

Based on STM observations of oxygen chemisorption and surface oxide formation a detailed description of the interaction of oxygen with Al(111) was derived.

The adsorption experiments were performed on substrate surfaces with a very low defect density, characterized by extended, atomically flat terraces and atomic steps. Atomic resolution images, often with both substrate and adsorbate atoms resolved, allowed a sensitive test of surface cleanness. Carbon as the only important contaminant

species was easily distinguished from adsorbed oxygen by its different appearance in STM images. Chemisorbed oxygen and surface oxide could be distinguished by STM, as for moderate tunnel currents and independent of the bias voltage the former are imaged as depressions, while the latter appear as protrusions. Pronounced changes, however, were noticed for the representation of adsorbed oxygen atoms by STM as the gap width was decreased, typically at tunnel resistances smaller than 10^8 Ω. Under these conditions individual oxygen atoms could be resolved. No evidence for a second, different chemisorbed oxygen species was found in these images.

Oxygen chemisorption was found to proceed randomly, with no preference for surface defects such as steps or carbon adatoms. An absolute coverage scale was established by counting individual O adatoms. The initial sticking coefficient for dissociative adsorption is determined to $s_0 = 0.005$, which is noticeable insofar as the earlier finding of dissociative oxygen adsorption even at 30 K rules out the presence of any significant activation barrier for this process. While the relative coverage-exposure relation resembles that of previous reports, both the absolute coverages as well as the initial sticking coefficient are significantly smaller than values reported previously. We conclude that oxygen coverages had been generally overestimated in previous studies.

Upon chemisorption at 300 K the O adlayer is characterized by randomly distributed, immobile, individual O adatoms and, at higher coverages, by small (1×1) O islands. These islands consist of few adatoms only. A quantitative evaluation at small coverages yielded a statistical distribution. From the random distribution of the thermalized, immobile O adatoms, with no indication of any pair correlation, a mobile, atomic precursor was concluded to exist, which results from an internal energy transfer from adsorption energy into kinetic energy parallel to the surface. These hot adatoms fly apart by at least 80 Å, before their excess energy is dissipated and they have thermalized. The minimum lifetime of this species was estimated to about 1 ps. This is in good agreement with results of a model calculation where energy transfer to the substrate occurs via electronic friction, though energy transfer via multiphonon excitation cannot be ruled out. The appearance of O_{ad} islands at coverages far below those necessary for statistical island formation indicates a preferential thermalization of precursor atoms upon collision with already thermalized adatoms or adatom islands. This points to a facile transfer of excess energy at the perimeter of thermalized O_{ad} atoms and islands, which agrees well with expectations based on the identical masses of the colliding species.

The onset of oxidation, evidenced by the appearance of new features in the STM images and of Al^{3+} in Auger spectra, begins at exposures around 60 L or coverages around $\Theta_0 = 0.2$, long before saturation of the (1×1) O adlayer. For a wide coverage range bare and O_{ad} covered areas coexist with the surface oxide. Oxide nucleation takes place at the interface of O_{ad} islands and bare surface, with a slight preference for nucleation at upper terrace step

edges. Further oxide formation progresses by nucleation of additional oxide grains rather than by growth of existing ones, until the surface is filled up with a layer of small oxide particles of about 20 Å in diameter. At very large exposures up to 10^5 L they cover the entire surface as a relatively smooth, amorphous layer of aluminum oxide. The difference in Al atom density between Al metal and surface oxide is accommodated by short range processes, with no indication for any long range mass transport.

Based on our data a two step model for the room temperature interaction of oxygen with Al(111) was discussed, which is much simpler than previous models insofar as it does not make use of an additional, chemisorbed subsurface oxygen species. In this model chemisorbed oxygen is formed in a first step, before in a second step oxide nuclei begin to form at the perimeter of existing O_{ad} island. With increasing exposure both phases grow simultaneously in coverage, until no bare surface is available any more. From this point on further oxygen uptake leads to conversion of O_{ad} areas to oxide nuclei, until finally the entire surface is covered by a closed layer of small oxide nuclei. The complex spectroscopic data of the O/Al(111) system are rationalized by the wide coexistence range of bare and O_{ad} covered surface with surface oxide and by differences in the electronic and vibronic properties of the surface atoms, depending on the local environment of these atoms: O adatoms or Al surface atoms with a different number of neighboring O adatoms are likely to exhibit significant differences in the above properties. This effect is particularly pronounced in this system because of the close proximity of the O adatoms in the (1×1) O islands, favoring large interaction effects, and because of the small island sizes, which lead to a large number of adatoms at the perimeter or edge of O_{ad} islands.

APPENDIX

The island density ρ [in islands per (1×1) adsorption site] and the oxygen coverage Θ [in oxygen atoms per (1×1) adsorption site] can be related on the basis of the following considerations (see Fig. 18): A hot adatom O^*, which moves across a surface partly covered by oxygen islands, can either thermalize on the bare surface or it is trapped by an island already present on the surface. In the first case a new island is formed and the number of islands increases by one, in the second case the number of islands remains constant. For simplicity the sticking probability for a precursor atom which hits an island is assumed to be unity. The possibility of back reflection and an influence of the kinetic energy of the O^* atom on its sticking probability are neglected. The rate $d\rho/d\Theta$ by which islands are formed with increasing coverage is therefore equal to the probability that the precursor does not hit an island: $d\rho/d\Theta = P$. P is a function of the island density ρ, of the trapping cross-section σ, and of the path length λ of the ballistic motion on the clean surface: $P(\rho, \sigma, \lambda)$. As illustrated in Fig. 18 the mobile atom O^* will be trapped by an island before it equilibrates on a clean part of the surface, if at
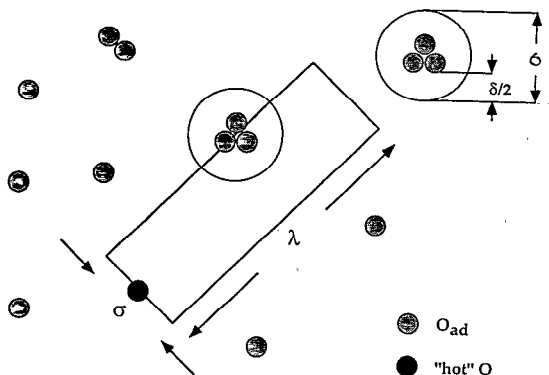
FIG. 18. Filled circle: hot oxygen adatom, shaded circles: thermalized oxygen atoms and islands. σ: cross section for a successful trapping event of the hot adatom at a thermalized island. $\delta/2$: zone of influence around an oxygen atom or island. λ: ballistic path length of the hot adatom.

least one island is located with its center inside a rectangle with side lengths σ and λ, where σ is composed of the island diameter d and the range of an attractive interaction δ. In turn, the probability P for not being trapped is equal to the probability that there is no island located inside this area, i.e., that none of the (1×1) sites inside the rectangle is occupied by an island center or an individual atom. This yields $P=(1-\rho)^{n}$, where n is the number of (1×1) sites in the area of the rectangle $\sigma\lambda$. With A the area of a (1×1) unit cell n is equal to $\sigma\lambda/A$, hence $d\rho/d\Theta=(1-\rho)^{\sigma\lambda/A}$. Finally we need an expression for the increase of the island diameter d with increasing coverage. Since the islands have compact shapes their geometrical diameter is about equal to the square root of the mean number of atoms per island $\sqrt{\Theta/\rho}$ times the lattice constant a. We then obtain $\sigma(\Theta) = a\sqrt{(\Theta/\rho)} + \delta$. This yields the following differential equation for the increase of the island density ρ with increasing coverage Θ:

$$\frac{d\rho}{d\Theta}=(1-\rho)^{\lambda/A(a\sqrt{(\Theta/\rho)}+\delta)}.$$

With $a=2.86$ Å, $A=7\times10$ Å^2, and $\delta=0$ (trapping only if O* hits O_{ad}, i.e., $\sigma=2.86$ Å for a single atom), numerical integration yields a good fit to the experimental data for $\lambda=160$ Å (lower curve in Fig. 16). For higher values of δ shorter drift lengths are obtained. For $\delta=2a$, equivalent to a cross section of three lattice constants for a single O_{ad} atom, a fit to the experimental data yields $\lambda=70$ Å (upper curve in Fig. 16).

[1] C. R. Brundle and J. Broughton, in *The Chemical Physics of Solid Surface and Heterogenous Catalysis*, Vol. 3A, edited by D. A. King and D. P. Woodruff (Elsevier, Amsterdam, 1990), p. 131.

[2] S. A. Flodström, C. W. Martinsson, R. Z. Bachrach, S. B. M. Hagström, and R. S. Bauer, Phys. Rev. Lett. 40, 907 (1978).

[3] J. Stöhr, L. I. Johansson, S. Brennan, M. Hecht, and J. N. Müller, Phys. Rev. B 22, 4052 (1980).

[4] D. Norman, S. Brennan, R. Jaeger, and J. Stöhr, Surf. Sci. 105, L297 (1981).

[5] A. Barrie, Chem. Phys. Lett. 19, 109 (1973).

[6] P. O. Gartland, Surf. Sci. 62, 183 (1977).

[7] I. P. Batra and L. Kleinman, J. Electron Spectrosc. Relat. Phenom. 33, 175 (1984).

[8] A. M. Bradshaw, P. Hofmann, and W. Wyrobisch, Surf. Sci. 68, 269 (1977).

[9] P. Hofmann, W. Wyrobisch, and A. M. Bradshaw, Surf. Sci. 80, 344 (1979).

[10] W. Eberhardt and F. Himpsel, Phys. Rev. Lett. 42, 1375 (1979).

[11] R. Payling and J. A. Ramsey, J. Phys. C 13, 505 (1980).

[12] R. Michel, J. Gastaldi, C. Allasia, J. Jourdan, and J. Derrien, Surf. Sci. 95, 309 (1980).

[13] J. L. Erskine and R. L. Strong, Phys. Rev. B 25, 5547 (1982).

[14] R. L. Strong, B. Firey, F. W. de Wette, and J. L. Erskine, J. Electron Spectrosc. Relat. Phenom. 29, 187 (1983).

[15] M. Kerkar, D. Fisher, D. P. Woodruff, and B. Cowie, Surf. Sci. 271, 45 (1992).

[16] C. F. McConville, D. L. Seymour, D. P. Woodruff, and S. Bao, Surf. Sci. 188, 1 (1987).

[17] P. S. Bagus, F. Parmigiani, G. Polzonetti, F. Illas, and C. R. Brundle, J. Vac. Sci. Technol. A 9, 1747 (1991).

[18] P. S. Bagus, C. R. Brundle, F. Illas, F. Parmigiani, and G. Polzonetti, Phys. Rev. B 44, 9025 (1991).

[19] H. Brune, J. Wintterlin, R. J. Behm, and G. Ertl, Phys. Rev. Lett. 68, 624 (1992).

[20] C. Gerber, G. Binnig, H. Fuchs, O. Marti, and H. Rohrer, Rev. Sci. Instrum. 57, 221 (1986).

[21] J. Wintterlin, J. Wiechers, H. Brune, T. Gritsch, H. Höfer, and R. J. Behm, Phys. Rev. Lett. 62, 59 (1989).

[22] G. Pötschke, J. Schröder, C. Günther, R. Q. Hwang, and R. J. Behm, Surf. Sci. 251/252, 592 (1990).

[23] V. M. Hallmark, S. Chiang, J. F. Rabolt, J. D. Swalen, and R. J. Wilson, Phys. Rev. Lett. 59, 2879 (1987).

[24] H. Brune, J. Wintterlin, G. Ertl, and R. J. Behm, Europhys. Lett. 13, 123 (1990).

[25] C. W. B. Martinsson, L.-G. Peterson, S. A. Flodström, S. B. M. Hagstrom, in *Proc. Int. Study Conf. on Photoemission from Surfaces*, edited by R. F. Willis, B. Feuerbacher, B. Filton, and C. Backx (Nordwijk, Holland, 1976), p. 177.

[26] R. Michel, C. Jourdan, J. Gastaldi, and J. Derrien, Surf. Sci. 84, L509 (1979).

[27] J. G. Chen, J. E. Crowell, and J. T. Yates, Phys. Rev. B 33, 1436 (1984).

[28] J. Wintterlin and R. J. Behm, in *Scanning Tunneling Microscopy*, Vol. 1, edited by H. J. Güntherodt and R. Wiesendanger (Springer, Berlin, 1992), p. 39.

[29] N. D. Lang, Comments Condens. Matter Phys. 14, 253 (1989).

[30] G. Doyen, D. Drakova, E. Kopatzki, and R. J. Behm, J. Vac. Sci. Technol. A 6, 327 (1988).

[31] E. Kopatzki, G. Doyen, D. Drakova, and R. J. Behm, J. Microsc. 152, 687 (1988).

[32] J. Tersoff and D. R. Hamann, Phys. Rev. B 31, 805 (1985).

[33] J. Harris and S. Andersson, Phys. Rev. Lett. 55, 1583 (1985).

[34] C. Astaldi, P. Geng, and K. Jacobi, J. Electron Spectrosc. Relat. Phenom. 44, 175 (1987).

[35] G. Ertl, S. B. Lee, and M. Weiss, Surf. Sci. 114, 515 (1982).

[36] A. L. Testoni and P. C. Stair, Surf. Sci. 171, L491 (1986).

[37] L. Kleinman and K. Mednik, Phys. Rev. B 23, 4960 (1981).

[38] E. Kopatzki and R. J. Behm, Surf. Sci. 245, 255 (1991).

[39] J. Harris and B. Kasemo, Surf. Sci. 105, L281 (1981).

[40] B. N. J. Persson, D. Schumacher, and A. Otto, Chem. Phys. Lett. 178, 204 (1991).

[41] E. V. Albano and V. D. Pereyra (submitted for publication).

[42] C. W. B. Martinsson, S. A. Flodström, J. Rundgren, and P. Westrin, Surf. Sci. 89, 102 (1979).

[43] V. Martínez, F. Soria, M. C. Munoz, and J. L. Sacedon, Surf. Sci. 128, 424 (1983).

[44] F. Jona and P. M. Marcus, J. Phys. C 13, L477 (1980).

[45] J. E. Crowell, J. G. Chen, and J. T. Yates Jr, Surf. Sci. 165, 37 (1986).

[46] P. Hofmann, C. v. Muschwitz, K. Horn, K. Jacobi, A. M. Bradshaw, K. Kambe, and M. Scheffler, Surf. Sci. 89, 327 (1979).

[47] P. Hofmann, K. Horn, A. M. Bradshaw, and K. Jacobi, Surf. Sci. 82, L610 (1979).

[48] C. W. B. Martinson and S. A. Flodström, Solid State Commun. **30**, 671 (1979).

[49] F. R. McFeely, J. F. Morar, N. D. Shinn, G. Landgren, and F. J. Himpsel, Phys. Rev. B **30**, 764 (1984).

[50] R. L. Strong, B. Firey, F. W. de Wette, and J. L. Erskine, Phys. Rev. B **26**, 3483 (1982).

[51] S. Andersson, Solid State Commun. **20**, 229 (1976).

[52] N. D. Lang, Surf. Sci. **127**, L118 (1983).

[53] D. M. Bylander, L. Kleinmann, and K. Mednik, Phys. Rev. Lett. **48**, 15 (1982).

[54] A. Büssenschütt, Diplomarbeit, Universität Hannover, 1990.